BEST AVAILABLE IMAGES

Defective images within this document are accurate representations of the original documents submitted by the applicant.

Defects in the images may include (but are not limited to):

- BLACK BORDERS
- TEXT CUT OFF AT TOP, BOTTOM OR SIDES
- FADED TEXT
- ILLEGIBLE TEXT
- SKEWED/SLANTED IMAGES
- COLORED PHOTOS
- BLACK OR VERY BLACK AND WHITE DARK PHOTOS
- GRAY SCALE DOCUMENTS

IMAGES ARE BEST AVAILABLE COPY.

As rescanning documents *will not* correct images, please do not report the images to the Image Problem Mailbox.

PCT WORLD INTELLECTUAL PROPERTY ORGANIZATION
International Bureau

INTERNATIONAL APPLICATION PUBLISHED UNDER THE PATENT COOPERATION TREATY (PCT)

(51) International Patent Classification 5 :		(11) International Publication Number:	WO 93/00046
A61B 6/02, 6/03	A1	(43) International Publication Date:	7 January 1993 (07.01.93)

(21) International Application Number: PCT/US92/05218

(22) International Filing Date: 19 June 1992 (19.06.92)

(30) Priority data:
717,840 20 June 1991 (20.06.91) US

(71) Applicant: BOARD OF REGENTS, THE UNIVERSITY OF TEXAS SYSTEM [US/US]; 201 West 7th Street, Austin, TX 78701 (US).

(72) Inventors: MCDAVID, W., Doss ; 400 Sagecrest, San Antonio, TX 78232 (US). DOVE, S., Brent ; 12418 Wandering Trail, San Antonio, TX 78284 (US). WELANDER, Ulf ; Ottev. 63, S-146 00 Tullinge (SE). TRONJE, Gunilla ; Iggesundsv. 52, S-122 41 Enskede (SE). WAGGENGER, Rogert, G. ; 132 South Laredo Highway, Lytle, TX 78052 (US). LEE, Michael, D. ; 7490 Brompton, #179, Houston, TX 77025 (US).

(74) Agent: BAHLER, David, D.; Arnold, White & Durkee, P.O. Box 4433, Houston, TX 77210 (US).

(81) Designated States: AT, AU, BB, BG, BR, CA, CH, CS, DE, DK, ES, FI, GB, HU, JP, KP, KR, LK, LU, MG, MN, MW, NL, NO, PL, RO, RU, SD, SE, European patent (AT, BE, CH, DE, DK, ES, FR, GB, GR, IT, LU, MC, NL, SE), OAPI patent (BF, BJ, CF, CG, CI, CM, GA, GN, ML, MR, SN, TD, TG).

Published
With international search report.
Before the expiration of the time limit for amending the claims and to be republished in the event of the receipt of amendments.

(54) Title: METHOD AND APPARATUS FOR COMPUTING TOMOGRAPHIC AND PANORAMIC SCANS

(57) Abstract

An apparatus and method for computing both tomographic and panoramic scans of an object (16). The apparatus (10) includes an X-ray source (12) and a linear x-ray detector (20), and is operable in two modes: a panoramic mode and a tomographic mode. In the panoramic mode, the detector (20) is aligned perpendicular to a plane of rotation, and the detector (20) and x-ray source are rotated together about an object (16) to be imaged, and about a center of rotation. In addition, the center of rotation travels along a predetermined path. The digital signals produced by the detector (20) are electronically processed to produce a panoramic x-ray image of the object (16). In the tomographic mode, the linear detector (20) is positioned to lie within the plane of rotation, and the detector (20) and x-ray source (12) are rotated together in the plane of rotation about a center of rotation and about an object (16) to be imaged. Signals produced by the detector (20) during rotation are electronically processed to produce a computed tomographic image of the object (16) being scanned. During the tomographic mode, the center of rotation can also travel along a predetermined path, and this eccentricity is mathematically corrected.

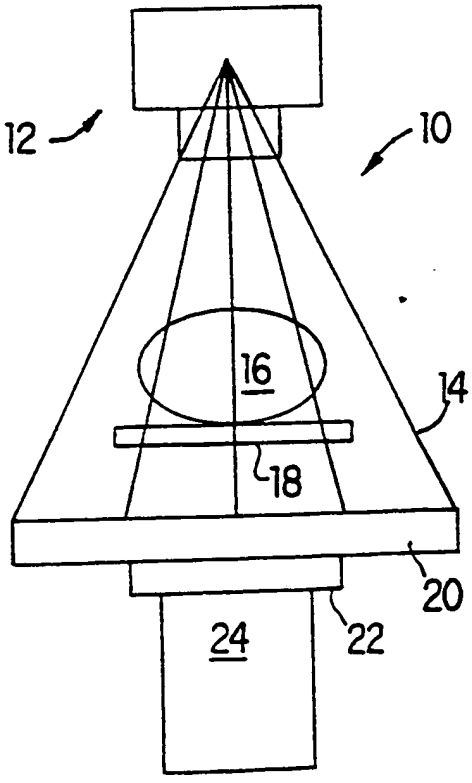

FOR THE PURPOSES OF INFORMATION ONLY

Codes used to identify States party to the PCT on the front pages of pamphlets publishing international applications under the PCT.

AT	Austria
AU	Australia
BB	Barbados
BE	Belgium
BF	Burkina Faso
BG	Bulgaria
BJ	Benin
BR	Brazil
CA	Canada
CF	Central African Republic
CG	Congo
CH	Switzerland
CI	Côte d'Ivoire
CM	Cameroon
CS	Czechoslovakia
DE	Germany
DK	Denmark
ES	Spain
FI	Finland
FR	France
GA	Gabon
GB	United Kingdom
GN	Guinea
GR	Greece
HU	Hungary
IE	Ireland
IT	Italy
JP	Japan
KP	Democratic People's Republic of Korea
KR	Republic of Korea
LI	Liechtenstein
LK	Sri Lanka
LU	Luxembourg
MC	Monaco
MG	Madagascar
ML	Mali
MN	Mongolia
MR	Mauritania
MW	Malawi
NL	Netherlands
NO	Norway
PL	Poland
RO	Romania
RU	Russian Federation
SD	Sudan
SE	Sweden
SN	Senegal
SU	Soviet Union
TD	Chad
TG	Togo
US	United States of America

METHOD AND APPARATUS FOR COMPUTING TOMOGRAPHIC AND PANORAMIC SCANS

The present invention relates to an apparatus and method for producing computed tomographic (CT) x-ray images as well as panoramic x-ray images.

X-ray computed tomography (CT) is a technique for obtaining cross-sectional reconstructions of three dimensional objects using x-rays. In the simplest example of CT imaging, a narrow beam of penetrating x-rays is scanned across an object or patient in synchrony with a radiation detector on the opposite side of the patient. If the beam is monoenergetic or nearly so, the transmission of x-rays through the patient is given by the equation

$$I = I_0 \exp(-\mu x) \qquad [1]$$

where the patient is assumed to be a homogeneous medium with the attenuation coefficient μ. If the x-ray beam is intercepted by two regions with attenuation coefficients μ_1 and μ_2 and thicknesses x_1 and x_2, the x-ray transmission is characterized as

$$I = I_0 \exp - (\mu_1 x_1 + \mu_2 x_2) \qquad [2]$$

This formula is generalized to many (n) regions with different linear attenuation coefficients with the argument of the exponent

$$\sum_{i=1}^{n} \mu_i x_i = (\mu_1 x_1 + \mu_2 x_2 + \ldots \mu_n x_n) \qquad [3]$$

$$I = \sum_{i=1}^{n} I_o \exp - (\mu_i x_i) \qquad [4]$$

Separate attenuation coefficients cannot be determined with a single transmission measurement because there are too many unknown values of μ_i in the equation. However, with multiple transmission measurements at different orientations of the x-ray source and detector, the separate coefficients can be distinguished so that a cross-sectional display of coefficients is obtained across the plane of transmission measurements. By assigning gray levels (see below) to different ranges of attenuation coefficients, a display is obtained that represents various structures in the patient with different x-ray attenuation characteristics. This gray scale display of attenuation coefficients constitutes a CT image.

The numbers computed by the reconstruction algorithm are not exact values of attenuation coefficients. Instead, they are integrals, termed CT numbers, which are related to attenuation coefficients. On most newer CT units, the CT numbers range from -1,000 for air to +1,000 for bone, with the CT number for water set at 0. CT numbers normalized in this manner are termed Hounsfield units and provide a range of several CT numbers for a one percent (1%) change in attenuation coefficients.

To portray the CT numbers as a gray scale visual display, a CRT is used. The CRT includes a contrast enhancement feature that superimposes the shades of gray available in the display device (i.e., the dynamic range of the display) over the range of CT numbers of diagnostic interest. Control of image contrast with the contrast enhancement feature is essential in x-ray computed tomography because the electron density, and therefore the x-ray attenuation, is remarkably similar for most tissues of diagnostic interest. These electron densities vary from 3.07×10^{23} elec/cc for fat tissue to 5.59×10^{23} elec/cc for the densest tissue, bone. Lung tissue has a much lower electron density, 0.83×10^{23} elec/cc, because of the alveolar and bronchial spaces.

The first CT systems were introduced in approximately 1971 by the EMI Corporation of England. These early systems used an x-ray source mounted in a gantry with detectors. The patient was inserted between the x-ray source and the detectors and the joined x-ray source and detectors were moved about the patient to obtain projection rays through the patient. These values were fed to a computer which then reconstructed a cross sectional image of the plane through which the pencil beam of x-rays passed. During this translational scan of perhaps 40 cm in length, multiple (e.g., 160) measurements of the x-ray transmission were obtained. Next, the angular orientation of the scanning device was incremented one degree and a second translational scan of 160 transmission measurements was performed. This process was repeated at one degree increments through an arc of 180 degrees so that 28,800 x-ray transmission measurements were accumulated. Those measurements were then transmitted to a computer equipped with a mathematical algorithms for reconstructing an image of

attenuation coefficients across the anatomical plane defined by the scanning x-ray beam.

Although this approach yielded satisfactory images of stationary objects, considerable time (4-5 minutes) was required for data accumulation and the images were subject to motion blurring. Soon after the introduction of pencil beam scanners, fan-shaped x-ray beams were introduced so that multiple measurements of x-ray transmission could be made simultaneously. Fan beam geometries, with increments of a few degrees for the different orientations (e,g., a 30-degree fan beam and 10-degree angular increments), reduced the scan time to 20-60 seconds and improved the image quality by reducing the effects of motion. Computed tomographic scanners with x-ray fan beam geometries and multiple radiation detectors constituted the second generation of CT scanners.

In late 1975, the third generation of CT scanner was introduced. These scanners eliminated the translational motion of previous scanners, using rotational motion of the x-ray tube and detector array or rotational motion of the x-ray tube within a stationary circular array of 600 or more detectors. With these scanners, data accumulation times as fast as two seconds are achievable.

Both stationary and rotating anode x-ray tubes are used in CT scanners. Many of the translation-rotation CT scanners have an oil-cooled, stationary anode x-ray tube with a focal spot on the order of 2 X 16 mm. The limited output of these x-ray tubes necessitates a sampling time of about 5 msec for each measurement of x-ray transmission. This sampling time, together with the time required to move and rotate the source and detector,

limits the speed with which data can be accumulated with CT units using translational and rotational motion.

To reduce the sampling time of 2-3 msec, most fast-scan CT units use rotating-anode x-ray tubes, often with a pulsed x-ray beam, to achieve higher x-ray outputs. Even with rotating-anode tubes, the heat-storage capacity of the anode may be exceeded if cooling periods are not observed between sets of successive images.

After transmission through the patient, the x-ray beam is collimated to confine the transmission to a slice with a thickness of a few millimeters and to reduce scattered radiation to less than one percent (1%) of the primary beam intensity. The height of the collimator defines the thickness of the CT slice. This height, when combined with the area of a single picture element (pixel) in the display, defines the three-dimensional volume element (voxel) in the patient corresponding to the two-dimensional pixel of the display. A voxel encompassing a boundary between two tissue structures (e.g., muscle and bone) yields an attenuation coefficient of the two structures. This "partial volume artifact" may be reduced by narrowing the collimator to yield thinner slices. However, this approach reduces the intensity of the x-rays incident upon the detector and the detector signals are subject to greater statistical fluctuations, thus introducing more noise in the displayed image.

To reduce the detector response time, all detectors used in CT scanning are operated in current rather than pulse mode. Also, rejection of scattered radiation is assigned to the detector collimator rather than to pulse height analyzers. Detectors for CT scanning are chosen on the basis of detection efficiency (greater than 50%),

short response time and stability of operation, and are either gas-filled ionization chambers or solid scintillation detectors. With any detector, the stability of response from one transmission measurement to the next is essential for the production of artifactfree reconstruction images. With a pure rotational source and detector geometry, for example, detector instability gives rise to ring-shaped artifacts in the image. Minimum energy dependence of the detector over the energy range for the CT x-ray beam also is important if corrections for beam hardening are to be applicable to all patient sizes and configurations.

All of the early CT systems were designed and built only to perform CT studies. The concept of using other types of radiation sources that had not been specifically designed for CT imaging was initiated in the mid 1970's.

Several of these efforts utilized existing x-ray therapy simulators. An x-ray simulator is a device that duplicates a radiation treatment unit in terms of its geometric, mechanical and optical properties, but uses a diagnostic x-ray tube as the source of radiation to simulate the properties of the treatment beam. A simulator allows the beam direction and the treatment fields to be determined while encompassing the target object with the simulator's irradiation. Since the simulator's emissions are generally less intense and less energetic than the emissions of therapy devices, there is a reduction in the target object's exposure to radiation.

The combination of a detector system and an x-ray therapy simulator provides the necessary front end of a CT system. Application of the requisite information processing techniques and algorithmic reconstruction

processes in combination with the simulator cum detector system enable production of CT images.

In conventional CT scanners, the x-ray source emits a scanned beam or fan of x-rays that lie in a plane, and the x-ray detector lies in the same plane. The x-ray source and detector are substantially fixed relative to one another, and are rotated together in the same plane that contains the x-ray detector and the x-ray beam. In contrast, in another type of radiography, known as panoramic radiography, the x-ray source and detector once again lie in the same plane, however, they are rotated in a plane that is transverse to the plane containing the source and detector. In certain panoramic x-ray devices, such as those used to produce panoramic images of the maxillo facial region, the center of rotation of the axis connecting the x-ray source and sensor moves along a curvilinear path while the sensor and detector are rotated about the center of rotation. During a panoramic scan, the detector, which is preferably a digital radiation detector, is periodically read, and the data is then conditioned to produce a digital panoramic x-ray image of the target object. In addition, and in contrast with conventional CT scanners, panoramic x-ray imaging devices typically scan only approximately 230° to 240° about the target object.

Reconstruction Algorithm

The first reconstruction formula was derived by an Austrian mathematician, P.J. Radon. Über die Bestimmung von Funktionen durch Ihre Integralwerte Laengs Gewisser Mannigfaltigkeiten, Berichte Sächsische Akadamie der Wissenschaffen (Leipzig), Mathematische-Physische Klasse 69, 262-277 (1917). His methods were based on the assumption of use of a parallel beam and concomitant data

collection. The fundamental process can be described as a convolution followed by a back projection. Subsequent methods derived from the Radon method utilized variations in the application of filters and convolution to correct for the effect of noise in the reconstruction process. Pavkovich and Nunan (U.S. Patents 4,149,248 and 4,365,339) modified Radon's algorithm to accommodate fan beam geometry. Their method consisted of a convolution of the original projection data with a function derived from the inverse Fourier transform (IFT) of a product of the Fourier transform of the projection data and the ramp function in frequency space. These results were then back projected to the point of interest, (X,Y). Their convolution was essentially an angular convolution for any given point. All of their mathematical manipulations were performed in configuration (real) space with no resort to transforms to frequency space.

Algorithms based upon the Radon method such as that developed by Pavkovich and Nunan suffer from two defects: (1) they are computationally burdensome, requiring both excessive memory and time of execution, and (2) they are very sensitive to noisy data; that is, resolution of the reconstructed image decreases disproportionately with increases in noise in the data. The Radon reconstruction method is theoretically perfect when operating on perfect data; that is, an infinite number of parallel, noiseless projections detected by an infinite number of detectors of infinitesimal dimension. These requirements unfortunately do not exist in physical systems. Using real data, results from the Radon method for calculating attenuation coefficients degenerate rapidly as the data becomes noisy and a finite number of discretely sized detectors is used.

Known reconstruction algorithms are of four general types:

(1) simple back projection (Radon);

(2) integral equations;

(3) Fourier transform; and

(4) series expansion.

In the present invention, the Fourier transform is utilized. In this approach, the x-ray attenuation pattern at each angular orientation is separated into frequency components of various amplitudes, similar to the way a musical note can be divided into relative contributions of different frequencies. From these frequency components, the entire image is assembled in "frequency space" and then reconstructed by an inverse Fourier transform reconstruction process into a spatially correct image.

While the various algorithms used for CT image reconstruction each have their own limitations, the quality of the overall procedure is dominated by the quantity and quality of the measured transmission data. The quantity of data is restricted by the specific scanner design and by limitations placed on time and computer resources. Phenomena which tend to degrade the quality of the measured data include:

a) Geometrical errors such as misalignment or motion of the scanning system or patient motion,

b) Instability of the x-ray source,

c) Statistical fluctuation of the measured signal,

d) Polychromaticity (non-monochromaticity) of the x-ray beam,

e) The finite dimensions of the scanning aperture,

f) Residual signal due to the time response function of the detector system (afterglow).

If, as a result of these factors, the projection values derived from the measured data do not adequately represent the line integrals of the linear attenuation coefficients within the slice being scanned, even the most perfect reconstruction algorithm will give rise to a distorted image. Each of these factors and the manner in which they are addressed in the case of the present invention is set out in the following paragraphs.

Geometrical Error

The most practical approach to error introduced by scanner misalignment or motion lies in the construction and maintenance of the scanner itself, including periodic testing of the mechanical registration. Patient motion is less controllable but can usually be minimized by proper patient support and through the use of the fast (fan beam) scanner. If patient motion is monitored, such as through the use of a transducer arrangement or a laser beam reflection method, then data correction is feasible. Using the method of the present invention, correction can even be made for eccentricity in the motion of the center of rotation; that is, when the center of rotation does not coincide with the center of reconstruction at a given range. Such eccentricity is measured and subsequently

corrected for all angles involved in the back projection and reconstruction.

In addition, the present invention can accommodate intentional eccentricity in the motion of the center of rotation, for example, when a panoramic x-ray apparatus is modified, in accordance with the present invention, to conduct CT scanning. In such CT scanning the center of rotation can intentionally move along a curvilinear path. Even such a gross eccentricity can be measured and subsequently corrected for all angles involved in the back propagation and reconstruction, in accordance with the present invention.

X-Ray Source Instability

The instability of the x-ray source is generally corrected for by adjusting the measured data in accordance with the signal measured by a reference detector. Another approach is to monitor the electronic parameters of the x-ray source, such as kVp and mA, and to make the corrections to the measured data from this information. The reference detector method, while not extremely sensitive to kilovoltage variations, is simpler and more easily utilized through electronic hardware. Computer correction in accordance with the present invention makes possible the use of lower cost x-ray power supplies and kVp monitoring to correct for changes in effective beam energy.

Statistical Fluctuation

Systemic error may arise in such forms as drift and gain variations in the detector system and associated electronics, or in the form of background or bias currents. If these variations can be monitored and

quantified, corrections can be implemented through hardware circuitry or computer correction.

Polychromatic Effects

Since flux-rate requirements based on statistical considerations for any reasonable scan time normally rule out the use of other sources of radiation, an x-ray tube is the only practical photon source for CT scanning. As a result, a spectral distribution of photons is involved rather than photons of a single energy. Since lower energy photons have higher attenuation coefficients than higher energy ones, the beam becomes progressively "harder" as it traverses an increasing patient thickness. A "harder" beam, having a lower effective attenuation coefficient than a "softer" one, introduces a degree of inconsistency into the measured data used for reconstruction. In the absence of compensation for this effect, e.g., utilizing a fixed length water bath or software corrections applied at the preprocessing stage, this effect leads to a distorted image characterized by a general increase in coefficients from the center to the periphery of the cross-section.

The object of preprocessing the measured transmission data before reconstruction is to "linearize" the logarithm of the ratio of the incident to transmitted intensity. For a monoenergetic beam traversing a homogeneous medium, this logarithm is a linear function of increasing thickness, while for a polychromatic beam this function is no longer linear. If the characteristic attenuation of a particular incident x-ray beam by an increasing mass thickness of water is known and if it can safely be assumed that the materials encountered within the body have attenuation properties similar to those of water, the measured data can be corrected to an idealized

monoenergetic (linear) response for some suitable energy. Since the corrected data is then logarithmically linear, that data can be utilized by the reconstruction algorithm to produce a spatially consistent image that is independent of patient size. This correction may also be implemented by assuming an average composition of tissue and bone instead of water for the various degrees of attenuation.

Finite Dimensions of Scanning Aperture

The qualities of resolution and image sharpness are closely associated with aperture size. Theoretical development of the reconstruction algorithms is based upon an infinite amount of infinitely thin transmission data which, in practice, is approximated by a finite number of transmission measurements of an x-ray beam of finite dimensions. The minimum aperture size is limited by photon statistics for a given x-ray output, geometry and scan speed.

The slit height, perpendicular to the linear motion of the scanner, acts to make the resultant reconstructed coefficient a type of average coefficient over many thin transverse planes. This average is not inconsistent with the assumption of infinitely thin rays since the theoretical development of these algorithms is limited to two dimensions. Distortions due to this vertical smearing are somewhat minimized because of the homogeneity of the human body over short vertical distances. In some respects, this smearing is advantageous in that a larger volume is considered in each cross-sectional slice, hence fewer slices need be reconstructed to include the entire volume of interest. However, in the two-dimensional reconstruction, the resultant coefficient need not pertain to only one type

of tissue, especially for small structures and near boundaries. This necessity is particularly important in relating these coefficients to effective atomic number, density, chemical composition, or specific tumor types.

The slit width, parallel to the linear motion of the scanner, introduces a compromise between the algorithm development and practical measurement. The approximation that the average intensity transmitted along the width of the aperture is the same as the relative intensity along a central ray is partially responsible for the lack of sharpness noted along many boundaries and can significantly degrade resolution. If the slit width is less than the linear increment between samples, computer enhancement of the data is not feasible. However, if the slit width exceeds this increment, then information is available from which the intensity for an aperture of a width approaching that of the linear increment can be calculated in accordance with the present invention. This technique is comparable to reconvolving the point spread function from other imaging devices, except the correction is applied to the measured data before an image is formed rather than as a modulation transfer function enhancement done as a post processing procedure on the final reconstructed image. The deconvolution is along discrete steps, the measured data, and not a continuum, therefore leading to the limit of data resolution, the linear increment.

Time Response of Detector System

The time response is an important consideration in the choice of detector systems. If signal decay due to an impulse of radiation on a detector is slow, then it would appear from the measurements alone that some radiation was still incident on the detector some short

time after radiation exposure. Likewise, a particular measurement during a scan may be partially due to radiation incident on the detector from some time prior to that measurement. In the case of the linear scanner considered here, this temporal smearing due to the detector response may be related to a type of spatial response of the detector by the time spacing of the measurements or scan speed. In this way, the time response of the detector is considered similar to or as part of the aperture transmission function and is corrected for in the same manner.

Applicability to Fan Beam Scanners

For fan beam scanners, many of these correction techniques still apply. Furthermore, the temporal response of the detector is related to measurements made with the same detector as a function of angle (time). The aperture itself is less likely to overlap than in the case of the linear scanner, however, the effective aperture due to cross-talk and patient scatter may also be handled by these preprocessing techniques. Modifications applicable to patient scatter may include making a correction to the measurement of interest as a function of intensity attenuated (including scatter) rather than intensity transmitted to a nearby detector along with the distance of this detector from the detector of interest. In any case, this type of scatter correction is just an approximation. The corrections pertaining to geometrical errors, instability of the x-ray source and the polychromaticity of the x-ray beam are applicable to either type of scanner.

Some of these techniques are known to be in commercial use, especially in regard to polychromatic correction. Hardware approaches to some of the problems

are also common, such as careful construction of the scanner and use of patient supports and restraints to minimize geometrical error, reference detector methods to compensate for x-ray source variation, temperature compensating amplifiers to reduce drift, increasing x-ray filtration to reduce polychromatic effect, increasing x-ray output to allow for smaller apertures, and the selection of detectors to reduce afterglow. Even so, the present method for reducing these factors which degrade the quality of the data is beneficial and in some cases, absolutely necessary.

In spite of these many improvements and alternative approaches, there remains a need for improved methods for reducing the effect of these error factors on a back projected image, as well as for actually back projecting the image of the target object. There is also a need for an apparatus for implementing these methods, and especially an apparatus which is capable of being mounted in combination with an existing x-ray simulator without changing the function of that apparatus.

In addition, several fields of medicine exist which use both CT scanning and panoramic imaging, typically requiring two separate machines. There is thus a need for a single x-ray apparatus capable of performing both CT scanning and panoramic imaging.

In accordance with a first aspect of the invention, the present invention solves the above-noted drawbacks of the prior art by providing an attachment for back projecting a CT scan using an existing x-ray simulator comprising a linear detector array, the mounting of which is adapted for mounting to the film holder of an x-ray simulator normal to the central axis of the fan beam produced by the simulator without altering the original

function of the x-ray source of the simulator, which comprises a plurality of individual elements. Each individual detector element produces an output signal having an amplitude proportional to the energy intensity of an x-ray incident thereon, the intensity of an incident x-ray being proportional to the density of the target through which the incident x-ray passes before striking the individual detector element. Also provided is means for collecting the output signals of each individual detector element at a plurality of incremental angles as said detector array and the source of the fan beam are rotated around the target object and translating the signals into a back projected computer tomographic scan of the target object.

Translation is accomplished by correcting for the spread of the x-rays in the fan beam and for the differences in the intensity of the x-rays comprising the fan beam depending on the position of the individual detector element in the detector array relative to the central axis of the fan beam. Translation also involves scaling the output signal to account both for the relative distance from the source of the fan beam to the detector array and for the distance from the fan beam source to the target object. The attachment also includes means for correcting the scaled signal for the magnification resulting from the spread of the fan beam and for transforming the output signal from each detector element into an output signal representing the output signal that would have been produced by each detector element had the incident x-ray originated from a parallel beam instead of a fan beam. Finally, translation involves converting the transformed output signal at each incremental angle of the detector array into a gray scale value for a picture element having a specific set of coordinates relative to the coordinates of the detector

array and outputting the gray scale value to an appropriate display means for displaying the tomographic scan.

Also provided is a method of producing a computed tomographic scan of a target object with an x-ray simulator comprising the steps of projecting an x-ray beam through a target object, detecting the x-ray beam incident on a detector positioned on the other side of the target from the source of the x-ray beam, defining polar and cartesian coordinate systems to describe the geometry of the x-ray beam, target object, and detector and locating the position of the source of the x-ray beam, the center of rotation axis, and the detector on the polar and cartesian coordinate systems for each incremental angle as the source of the x-ray beam and the detector rotate relative to the center axis of the target object. The output signal from each detector is then transformed into an output signal representing the output signal which would have been produced by that detector had the incident x-ray originated from a parallel beam source rather than a fan beam x-ray source and the transformed output signal is converted at each incremental angle of the detector into a gray scale value for a picture element having a specific position on the cartesian coordinate system. The gray scale values are then output to an appropriate display device.

In accordance with another aspect of the present invention, CT scanning capabilities and panoramic imaging capabilities are combined into a single apparatus capable of operating in two distinct modes, with only minor modifications to the hardware. In a first mode of operation (the panoramic mode), the x-ray source and sensor are aligned in a plane, and are rotated together in a transverse plane. If desired, the center of

rotation can also be translated along a predetermined curvilinear path, in order to follow the portion of anatomy being imaged, for example, the maxillo facial region. In a second mode of operation (the CT scanning mode), the detector and x-ray source are aligned in the same plane as the plane of rotation. In accordance with the present invention, the eccentric movement of the center of rotation can be accommodated so that an undistorted CT image is produced.

Figure 1 is a schematic, sectional view of an x-ray simulator having an apparatus constructed in accordance with the present invention mounted thereto.

Figure 2 is a schematic of the component parts of the apparatus of the present invention and the processing of the data by those parts.

Figure 3 is a flow chart of the processing of the data in accordance with the method of the present invention.

Figure 4 is a schematic representation of the geometry of the coordinate system in which the x-ray source, target, and detector array of the present invention are located.

Figure 5 is a schematic representation of the geometry of the back projected image computed in accordance with the method of the present invention.

Figure 6 is a graphical representation of an exaggeration of a measured center of rotation shift for an x-ray simulator rotating 360°. The off-center shift S_j is plotted as a radius from the center versus the angle in degrees.

Figure 7A is a graphical representation of a method for measuring the center of rotation shift as a function of an angle j.

Figure 7B is a schematic representation of one type of error in data acquisition and back projection, which results in distortion and blurring of the back projected image of a phantom, as a result of the superposition of translational and rotational movement of the x-ray source of a panoramic x-ray device with respect to the phantom. For purposes of clarity, only two rays P_1 (shifted to P_1+5) and P_2 (shifted to P_2+5) are shown having been shifted by this eccentric rotation.

Figure 8 is a schematic representation of the divergence of a ray emanating from a point source and the different magnification factors that result as the ray passes through the object.

Figures 9A and 9B show alternative methods using the spacing element δr which is utilized during back projection as either a constant value (Fig. 9A) for the horizontal back projection or a variable value (Fig. 9B) for the back projection from the detector line.

Figure 10 is a representation of the rectangular pixel grid containing the circle of image reconstruction and showing the sum of the back projection geometrical factors at each pixel in the 16 x 16 grid.

Figures 11A and 11B illustrate the filters used for processing the output signals of the detector elements and the effect of each type of filter on the convolved projection data, respectively.

Figure 12 is another schematic representation of the geometry of the coordinate system in which the x-ray source, target, and detector array are located in accordance with the present invention.

Figure 13 is another flow chart of the processing of the data in accordance with the method of the present invention derived from the geometry of Figure 12.

In accordance with a first embodiment of the present invention, and referring to Fig. 1, there is shown a schematic representation of an x-ray simulator, indicated generally at reference numeral 10. X-ray simulator 10 is generally comprised of the x-ray tube 12 used for radiation therapy simulation which produces a fan beam, indicated at reference numeral 14, incident upon a target object 16 positioned on table 18. X-ray beam 14 is also incident upon the detector array (not shown) of the apparatus 20 of the present invention. The apparatus 20 is comprised of the linear detector array 26 (see Fig. 2), the mounting of which is adapted for fitting into, mounting next to, or covering the film holder 22 of x-ray simulator 10 normal to the central axis of the fan beam 14 produced by the source 12 without altering the original function of simulator 10. The film holder 22, or cradle, is mounted on top of the image intensifier tube 24. The x-ray beam is collimated by using the shutters or collimators (not shown) provided by the x-ray therapy simulator 10. The beam 14 is preferably shaped with a width of approximately one centimeter and a spread determined by the length of the detector array 26 of the apparatus 20 of the present invention. If the projected shadow of the target object 16 to be scanned is less than the maximum width of the detector array 26, the spread of the beam 14 is decreased so as to just encompass the diameter of the target object 16.

Fig. 1 is shown as a schematic representation of a conventional x-ray simulator which rotates around a target object (as will be explained below) in a 360° arc for reconstructing an image. However, those skilled in the art who have the benefit of this disclosure will recognize that reconstruction can also be accomplished using projections from an arc of rotation that is less than 360°; for example, by using a dental panoramic x-ray unit which rotates through an arc of approximately 230-240°. It is specifically contemplated that the apparatus 20 can be mounted to, and the method of the present invention can be accomplished in connection with such dental panoramic units as, for instance, the AUTOPAN (Belmont Equipment Co., Summerset, N.J.), GX-PAN or PANELIPSE II (Gendex Corp., Milwaukee, WI), PANOREX II (Keystone Corp., Neptune, N.J.), or, in a presently preferred embodiment, the Siemens Medical Systems (Charlotte, N.C.) OP 10 dental x-ray unit. Additional detail regarding the use of the present invention in combination with panoramic machines is discussed in detail below with reference to Figs. 12 and 13.

Referring now to Fig. 2, there is shown a schematic representation of an exemplary apparatus used in connection with the method of the present invention. The detector array 26 utilizes an image intensifying screen (not shown in Fig. 2) placed over a linear photodiode array of detectors. In a presently preferred embodiment, the photodiode array is comprised of eight to sixteen (or more) light sensitive modules (not shown), each composed of a silicone chip with 127 photodiodes (not shown) such as the Model THX-1086 (Thompson Electron Tubes Division, CSF Thomson et Cie (Paris, France). The photodiodes are used in a capacitive storage mode (with reverse bias) so that the light emitted by the intensifying screen discharges the photodiode capacitors. The scintillator

material used is ytterbium-gadolinium oxide, a screen material commonly used in diagnostic radiology. Other scintillator materials may likewise be used to advantage, and the screen may be made of different thickness to improve photon collection efficiency.

An external sync trigger circuit 28 is provided for interfacing the x-ray simulator 10 with an external sync circuit 30 to trigger the timing circuitry of the apparatus 20 of the present invention when the x-ray tube 12 starts to emit the fan beam 14. External sync circuit 30 provides the synchronization signal to the preprocessor 32 and determines the integration period of the detector array 26. The external sync circuit 30 consists of an input (not shown) to provide software control of offset and gain calibration reset signals to the preprocessor 32, a continuous clock circuit (also not shown) to provide the synchronization and integration period for the detector array 26 during gain calibrations, and a variable clock circuit (also not shown) which utilizes an EPROM to provide the synchronization and integration period for the detector array 26 during data acquisition. The preprocessor 32 receives the analog signal from the detector array 26 and, under control of the external sync circuitry 30, digitizes and outputs the data to the microcomputer interface circuit 34.

Computer interface circuit 34 converts the data received from the preprocessor 32 to a format compatible with the input-output (I/O) board 36 of the particular microcomputer utilized for processing the data as described below. The microcomputer I/O board 36, after receiving the data from microcomputer interface circuit 34, inputs the data to the memory of the microprocessor 38, which is preferably a Motorola 68030 or Intel 80386-

based computer. In a presently preferred embodiment, an Apple Mac II Plus (tm) with eight megabyte memory, large hard disk, 80-140 megabytes, floppy disk and CRT displaying a 480 x 512 pixel image (or, alternatively, a special CRT to display a 512 x 512 image) having a 25 and preferably 30 megahertz internal clock is used to advantage. In addition, the output of the microcomputer I/O board 36 provides the software control signals to the external sync circuit 30 for offset and gain calibrations, the continuous clock and variable clock circuits. The microcomputer 38 performs the data manipulation routines described below to produce the CT image, outputting the processed data to an appropriate high resolution monitor 40 which provides a gray scale or color display of the reconstructed CT image, the film recorder (matrix camera) 42 which provides a hard copy output (film) of the image on the high resolution monitor 40, and/or the large capacity storage device 44 which stores the image data as well as patient information.

A general schematic outline of the data manipulation process is set out in Fig. 3. By the term "data" it will be understood that reference is made to the processed output signals of each individual detector or photodiode comprising detector array 26, which is proportional to the intensity of the x-ray incident thereon. Preprocessor 32 integrates the output signal of each photodiode and reads out the resultant signal upon external command controlled by microcomputer 38. In so doing, the data is corrected, smoothed, and filtered as shown in the step represented by box 46 in Fig. 3. This filtering step is required because the individual detector elements, or photodiodes, become defective and may malfunction either partially or completely. A correction algorithm is provided which identifies those faulty detector elements through comparison with the

neighboring detector elements (the narrow separation between detector elements utilized allows the generalization that the response for adjacent detector elements should be relatively close to each other), and replaces the bad data with a corrected, interpolated value. A smoothing algorithm is provided for extending this method by setting a limit, or preset selection criterion, on the variation of adjacent individual detector elements and interpolating response values for those detector elements whose variation from the neighboring detector elements exceeds that preselected criterion. Recognition of when an individual detector element malfunctions is determined experimentally by exposure to x-rays both in air and through a phantom target (not shown) and the history of the detector array.

Characterizing each step in more detail, the data is first smoothed in accordance with the formula

$$P(2) = (P(1) + P(3))/2 \qquad [1]$$

where P(1), P(2), and P(3) represent the signal outputs from each of three successive detector elements in detector array 26. The smoothing is extended by selecting a maximum variation between adjacent detectors based upon the detector response history. For example, a cutoff limit of ± 0.2 or 0.3 times the adjacent value may be selected so that if the reading from a particular detector element varies from its neighbors by more than 0.2 or 0.3 times the output of the neighboring elements, that output signal is replaced by the average of the output signal from the neighboring elements on either side of the bad element. In the event that several detectors in a row have malfunctioned, a scaled averaging method is used to correct the data. The difference between the last good output signal at one end of the

malfunctioning row of detector elements and the first good output signal at the other end is divided by the number of detector elements malfunctioning and the resultant quotient is used as a constant which is sequentially and iteratively added to the last good output signal to provide a replacement for the next output. The correction is added to this value for the next reading and so on, up to the first good output signal. For example, given the following output signals, 110, 125, 255, 255, 255, 255, 140, 141, the correction is applied as follows:

$$C = (140 - 125)/5 = 3 \qquad [2]$$

In this example, there are five intervals from the last good output signal at one end of the malfunctioning detector elements and the first good output signal on the other end of the malfunctioning detector elements. The corrected output data is 110, 125, 128, 131, 134, 137, 140, 141.

Other corrections account for variations in x-ray output. These variations can be caused by current and/or voltage variations. Metering circuits on the x-ray simulator 10 are used to monitor these parameters, and the output of those circuits is used as an input to processor 32. Current variations are corrected in linear fashion: if, for instance, the current drops from 5 mA to 4 mA, the detector elements are corrected as (5/4) x P(i). Voltage corrections are non-linear. The correction factor is formed as a power function of the voltage, i.e., V^N, where N is a number in the range $1.5 \leq N \leq 3$. N is determined experimentally and is idiosyncratic to the system being controlled. Suppose the voltage drops from 120V to 110V and, for that range,

it has been determined that N = 2. The correction is made as follows:

$$P(i)_{corr} = [120/110]^2 \times P(i) \qquad [3]$$

Additional corrections are performed using interpolation procedures to optimize accuracy in the calculated intensities used in back projection when correlating the detector in the detector array 26 that intercepts a back projected, or parallel beam, ray 50 (Fig. 4) which passes closest to the point in the target object 16 being reconstructed. The coordinate system in the back projection process is defined from i = 0 at the first (-x) detector to $N_D - 1$, where N_D is the number of detectors in the array 26. For example, using a 2048 detector array 26 with a detector spacing of x = 0.045 cm, the total length D_L of the line of detectors in detector array 26 is

$$D_L = (2048) \times 0.045 \text{ cm} = 92.16 \text{ cm}. \qquad [4]$$

The factor 2048 is used because the detector line is based on the spacing of the individual detectors and there are 2047 spaces between the 2048 individual detectors in a presently preferred embodiment of detector array 26. It should be understood that detector arrays with other numbers of individual detectors (for example 1048) may also be used. The center of the detector line is taken as zero. The x coordinate along this line then varies from -92.16/2 to 92.16/2, and the x coordinate of the i^{th} detector is

$$x_i = -46.08 \text{ cm} + (i + 0.5) \times 0.045 \text{ cm}, \qquad [5]$$

e.g., for the 1135^{th} detector,

$$x_{1135} = -46.08 + (1135 + 0.5) \times 0.045 = 5.0175 \text{ cm.}$$

The coordinate on the detector line where the ray passes closest to the reconstruction target point is designated L_{bp} (back projected). Once this coordinate is determined, it is possible to calculate which individual detector will receive the ray passing through L_{bp}. Let

$$N_{bp} = \text{int}[(L_{bp} + 46.08)/\delta x) + 0.5] \qquad [6]$$

where "int[]" indicates the integer part of the number in the brackets in equation [6] and the factor 0.5 is an end correction such that in the limit where L_{bp} is approximately equal to -46.08, the formula will return the integer value of one (1).

Round off error in calculating this integer is minimized by linear interpolation. The fractional part of N_{bp} is

$$N_{bp} - [N_{bp}] = f_{bp}. \qquad [7]$$

In the simplest round off, i.e., if $f_{bp} < 0.5$, $N_{bp} = [N_{bp}]$. If $f_{bp} \geq 0.5$, $N_{bp} = [N_{bp}] + 1$. For example, if $N_{bp} = 756.528$, the detector output taken would be P1(757). To be more exact, interpolation yields

$$P1 = (1 - f_{bp})\ P1([N_{bp}]) + f_{bp}\ P1([N_{bp}] + 1).$$

In the numerical example, P1 = (1 - .528) P1(756) + .528 P1(757).

The term "smoothing" (steps 46 and/or 72 of Fig. 3) refers to the filtering of the data by both smoothing and

ripple filtering. Smoothing is accomplished using a set of reconstructed values which may be represented as

$$\begin{matrix} M(1,1) & M(1,2) & M(1,3) & \ldots\ldots\ldots & M(1,N) \\ M(2,1) & M(2,2) & M(2,3) & \ldots\ldots\ldots & M(2,N) \\ M(3,1) & M(3,2) & M(3,3) & \ldots\ldots\ldots & M(3,N) \\ & & \vdots & & \\ M(N,1) & M(N,2) & M(N,3) & \ldots\ldots\ldots & M(N,N) \end{matrix} \quad [8]$$

Here, $N = 2^k$ where k = an integer, i.e., N = 128, 256, 512, etc. For four point smoothing for nearest neighbor (j denotes the row and i denotes the column):

$$M(j,i) = [M(j-1,i)+M(j+1,i)+M(j,i-1)+M(j,i+1)]/4 \quad [9]$$

The top, bottom, and adjacent left and right neighbors are used with equal weight. For five point smoothing for nearest neighbor,

$$M(j,i)=[M(j,i)+M(j-1,i)+M(j+1,i)+M(j,i-1)+M(j,i+1)]/5 \quad [10]$$

M(j,i) is added in along with the four nearest neighbors. For weighted neighbor smoothing with the central value given the greatest weight, nine point smoothing is used:

$$\begin{aligned} M'(j,i) = [&1xM(j-1,i-1) + 2xM(j-1,i) + 1xM(j-1,i+1) \\ &+ 2xM(j,i-1) + 4xM(j,i) + 2xM(j,i+1) \\ &+ 1xM(j+1,i-1) + 2xM(j+1,i) + 1xM(j+1,i+1)]/16. \end{aligned} \quad [11]$$

This weighting system can be varied with different weights applied to different locations depending upon the circumstances as known to those skilled in the art.

Ripple filters are used to eliminate the wave introduced into the reconstruction by employing Fourier methods. The first step in application of such a filter is to obtain x-ray transmission values for a water (uniform target density) phantom. With known reconstructed CT values, these true values are compared to observed CT values. The ripple filter factor for each picture element is given by the true value/observed value. To achieve correction, the value for each picture element is multiplied by the filter factor. There are many other different types of filters which may be used to advantage depending upon the circumstances as known to those skilled in the art who have benefit of this disclosure. Such filters might include, for instance, edge enhancement filters, high frequency suppression, bone enhancement filters, soft tissue enhancement filters, and so on.

The smoothed, corrected data from step 46 is convolved at step 47 and then back projected at step 48. Convolution 38 and back projection 48 are accomplished in accordance with an algorithm which is derived as follows. Referring to Fig. 4, there is shown the geometry for the fan beam 14, the parallel beam 50 and the coordinate system used to describe the algorithm of the present invention. In this system, the origin is established at the nominal center of rotation 56 with the knowledge that the nominal center may vary during the rotation. The x-axis 52 is on a line 54 through the center of rotation 56 so that the +x axis will coincide with the left side of the target object 16 and perpendicular to the y-axis 58 which passes through the center of rotation 56 on a line from the x-ray source 12 to the center of the detector array 26 (which is parallel to the x-axis 52), with the +y axis oriented toward the front of target object 16. As shown in stick figure in Fig. 4, if target object 16 is a patient, the +z axis is oriented toward the patient's head; the coordinate system, when

defined in this manner, is a right-handed system. The x-ray source 12, is assumed to rotate counterclockwise about the z axis with the angle of the x-ray defined from the +x axis, and the starting point of rotation is assumed to be 90°, or the x-ray target coinciding with the +y axis. In this fashion, images will be reconstructed that show the right side of the subject on the left side of the image and reflect the viewpoint of looking at the image from the foot of the patient toward the head.

The distance from the x-ray source 12 to the center of rotation 56 is D, reference numeral 60. The separation between the center of rotation 56 and the plane of the detector array 26 is a distance V, reference numeral 62. The x-ray source 12 and detector array 20 are incrementally rotated about the center of rotation 56 through angles T as shown at reference numeral 64 in Fig. 5. The increments may be equal in size or unequal. When equal increments are used, $T = 180°/N$ or $T = 360°/N$, where N is the number of increments, and the system may be rotated either through a semi-circle or the entire arc of a circle. Rotation through the arc defining a semicircle is commonly used in dental panoramic x-rays, and the coordinate system defined above is equally applicable in that instance. However, additional detail is also provided below with reference to Figs. 12 and 13. In such apparatus, the center of rotation 56 is not fixed such that both D and V vary at each angular increment. As set out below, the change in the location of the center of rotation 56 is measured and, using the method of the present invention, the back projection is corrected for the resulting known error.

For equal increments, the index, j, will nominally run from 0 to 359 or from 0 to 719 depending upon whether the projections are taken at one degree or 0.5 degree intervals. The number of angles used for acquisition of

data is limited by the ability of the data collection system and the computer system to acquire and process the given volume of input data. The increment between angles T_j and T_{j+1} is denoted by δT and is given by 360/N or 720/N.

The projection angle, T_j, indicated at reference numeral 66, is given, in the equal increment case, by

$$T_j = 90° + j\delta T \text{ where } 0 \leq j \leq N - 1. \quad [12]$$

The x-ray source coordinates for each j are given by

$$x_s(j) = D_s(j)\cos T_j \quad [13]$$

$$y_s(j) = D_s(j)\sin T_j. \quad [14]$$

Since the origin of coordinates is at the center 56 of the target 16, the nominal distance of the x-ray source to the origin is

$$D_s(j) = [x_s^2(j) + y_s^2(j)]^{1/2}.$$

The coordinates, $x_s(j)$ and $y_s(j)$ must be known for all angles T_j. The x-ray source and detector array are assumed to be rigidly connected and co-moving in the rotation about the target 16. As described above, the angle $T_0 = 90°$ defines the initial configuration of the system before rotation, e.g., at $j = 0$. At this angle, T_0, the coordinates of each of the detectors in detector array 26 are:

$$x_d(0,i) = - D_L/2 + (i + 0.5)\ \delta i \quad [15]$$

$$y_d(0,i) = - V \quad [16]$$

where $\delta i = D_L/N_d$, D_L is the length of the detector line, and N_d is the number of detectors in array 26 where $0 \leq i \leq N_d$.

Equations [15] and [16] describe the coordinates for non-eccentric motion; as described above, when motion is eccentric, both x and y can be measured and input or solved for iteratively. The 0th detector is considered the left most detector on the -Y axis, and the spacing is actually the distance between the centers of each detector in detector array 26. The factor 0.5 in equation [15] serves to define the end point of the ray in the center of the detector element. For $T_j > 90°$, the coordinates of each detector in detector array 26 are given by:

$$x_d(j,i) = x_d(0,i) \cos(j\delta T) - y_d(0,i) \sin(j\delta T) \quad [17]$$

$$y_d(j,i) = x_d(0,i) \sin(j\delta T) + y_d(0,i) \cos(j\delta T). \quad [18]$$

In Figure 4, the parallel rays 50 are constructed by back projection from the detector array 26. The intersections of the parallel 50 and fan beam 14 rays define the circle of reconstruction 68.

In defining the circle of reconstruction 68, the next step 70 (see Fig. 3) in manipulation of the data is accomplished by microprocessor 38 using the following steps. The diameter D_{rc} of the reconstruction circle 68 along the line 54 is given by the scaling relationship

$$D_{rc}/D = D_L/W. \quad [19].$$

The radius of reconstruction circle 68 is $R_{rc} = D_{rc}/2$ and $W = D + V$ defines the distance from the x-ray source 12 to the center of the detector array 26. The Jacobian of the

scaling transformation from the detector array 26 to the line 54 along the diameter of reconstruction circle 68 is

$$M_1 = D/W \qquad [20]$$

The scaling factor M_1 allows transformation of the data taken along the detector line to appropriate values along the parallel line 54 through the center of rotation 56 and lying along a diameter of the reconstruction circle 68.

The distance between successive back projected parallel beams or detector rays 50 at the level of the diameter of the reconstruction circle 68 is the same as the individual detector aperture projected back to the center of rotation as a length

$$\delta R = \delta i \; M_1. \qquad [21]$$

The scaling factor may be written explicitly for each row 100 (see Fig. 8) of pixels in reconstruction circle 68. The individual detector aperture projects back to the center of rotation as a length

$$d_r = [D/W]\delta i \qquad [22]$$

An index c is defined such that c = 0 indicates the top row 100 of picture elements in the reconstruction circle 68 and $c = N_p - 1$, e.g., c_{15} at reference numeral 104 in Fig. 8, indicates the bottom row. Similarly, the index b used in equation [38] below indicates the columns 102 of pixels in the reconstruction circle 68. Here, b = 0 indicates the left most column. The magnification M_1 defined for the row

through the center of the reconstruction circle 68 is generalized as

$$Magp(c) = [D - y(c)]/W \qquad [23]$$

where $y(c) = D - R_{rc} + (c + 0.5)\ D_{py}$.

D_{py} is the height 106 of the picture element of row c and D_{px} is the width 108 of the picture element of row c. The row of pixels lying on the diameter of the reconstruction circle 68 therefore have width and height given by

$$D_{px} \text{ or } D_{py} = D_{rc}/N_p \qquad [24]$$

where N_p^2 = number of reconstruction pixels; i.e., 256, 512, etc.

To normalize the projected data from the incident beam, fan beam projection data is taken for x-ray transmission through air and through target objects. Let

$$P(j,i) = \log\ (r_{a(j,i)}/r_{p(j,i)}) \qquad [25]$$

where $r_{a(j,i)}$ is the ith detector reading at angle T_j in air and $r_{p(j,i)}$ is the ith detector reading at angle T_j for x-rays transmitted through the patient or other target 16. The ranges of the integer indices are as defined above.

Projection data for each angle T_j has been defined as p(j,i). This function is re-written in terms of the spatial variable s and angle ϕ in the reconstruction circle

68 as $p(s,\phi)$. The one dimensional Fourier transform of $p(s,\phi)$ at a given angle ϕ is written as

$$[\mathcal{F}p](S,\Phi) = \int_{-\infty}^{\infty} p(s,\phi)\ \exp[-2\pi iSs]\ ds \qquad [26]$$

In the discrete form, for each angle T_j, the one dimensional Fourier transform of the projection data is

$$[\mathcal{F}p](S,\Phi) = \sum_{k=0}^{N_D-1} p(k,\phi)\ \exp[-2\pi iSs(k)] \qquad [27]$$

where $s(k) = -R_{rc}+(k+0.5)\delta s$. Recall that $\delta s = 2R_{rc}/N_D$ and δs = the increment between adjacent rays in the spatial domain where s is the spatial domain variable, S is the frequency domain variable, $i = \sqrt{-1}$ in this equation and $s = 1/S$. In this application, s is expressed along the line R (65 in Fig. 5) in the reconstruction circle 68, and R is displaced on angle ϕ, measured counterclockwise from the +x axis. Integration is taken over the entire real domain where $-\infty < S < \infty$.

The one dimensional Fourier transform of the function $p(s,p)$, written only as a function of s for a given ϕ, is defined in the continuous notation by

$$[\mathcal{F}p](S) = \int_{-\infty}^{\infty} p(s)\ \exp[-2\pi iSs]\ ds. \qquad [28]$$

It is necessary to perform a two dimensional inverse Fourier transform to obtain the linear absorption coefficients, $\mu(x,y)$, describing target optical densities. Coordinates (x,y) are used in the Cartesian spatial domain containing the reconstruction circle 68 but defined by the

68 as $p(s,\phi)$. The one dimensional Fourier transform of $p(s,\phi)$ at a given angle ϕ is written as

$$[\mathcal{F}p](S,\Phi) = \int_{-\infty}^{\infty} p(s,\phi)\ \exp[-2\pi iSs]\ ds \qquad [26]$$

In the discrete form, for each angle T_j, the one dimensional Fourier transform of the projection data is

$$[\mathcal{F}p](S,\Phi) = \sum_{k=0}^{N_D-1} p(k,\phi)\ \exp[-2\pi iSs(k)] \qquad [27]$$

where $s(k) = -R_{rc}+(k+0.5)\delta s$. Recall that $\delta s = 2R_{rc}/N_D$ and δs = the increment between adjacent rays in the spatial domain where s is the spatial domain variable, S is the frequency domain variable, $i = \sqrt{-1}$ in this equation and $s = 1/S$. In this application, s is expressed along the line R (65 in Fig. 5) in the reconstruction circle 68, and R is displaced on angle ϕ, measured counterclockwise from the +x axis. Integration is taken over the entire real domain where $-\infty < S < \infty$.

The one dimensional Fourier transform of the function $p(s,p)$, written only as a function of s for a given ϕ, is defined in the continuous notation by

$$[\mathcal{F}p](S) = \int_{-\infty}^{\infty} p(s)\ \exp[-2\pi iSs]\ ds. \qquad [28]$$

It is necessary to perform a two dimensional inverse Fourier transform to obtain the linear absorption coefficients, $\mu(x,y)$, describing target optical densities. Coordinates (x,y) are used in the Cartesian spatial domain containing the reconstruction circle 68 but defined by the

axis along the center of the projected x-ray beam and the orthogonal detector array. The equivalent coordinates in the frequency domain are (X,Y). The projection at angle T_j for detector array element i, p(j,i), is expressed as a function of the new coordinates. Thus, p(j,i) is written as p(x,y) in the spatial domain and P(X,Y) in the frequency domain. In practice, the one dimensional transformation along the line s is equivalent to the two-dimensional transformation for points on the same line at the angle ϕ. Thus, the inverse Fourier transform, $\mathcal{F}^{-1}$ in this notation, is

$$[\mathcal{F}^{-1}P](x,y) = \int_{Y_{-m}}^{Y_m} \int_{X_{-m}}^{X_m} P(X,Y)\ \exp[2\pi i(xX + yY)]\ dXdY \qquad [29]$$

where $X_{\pm m}$, $Y_{\pm m}$ are the upper and lower bounds where P(X,Y) exists.

In the polar coordinates (S,Φ), this equation becomes

$$[\mathcal{F}^{-1}P](s,\phi) = \int_0^{2\pi} \int_0^{Sm} P(S,\Phi)\ \exp\ [2\pi i(xS\cos\Phi + yS\sin\Phi)]|S|dSd\Phi \qquad [30]$$

The limits in the integrals are rearranged to

$$[\mathcal{F}^{-1}P](s,\phi) = \int_0^{\pi} \int_{-S_m}^{Sm} P(S,\Phi)\exp[2\pi i(xS\cos\Phi + yS\sin\Phi)]|S|dSd\Phi \qquad [30]$$

Note the appearance of |S|, the ramp function, as a result of applying the Jacobian to transform the coordinate systems. The ramp function acts a filter. Here, the frequency is determined by the sampling theorem, which

states that where a function h(s) is defined over the range $2R_\pi$ (diameter of the reconstruction circle 68) then the Fourier transform of h(s), H(S), is fully described by points $\delta S = 1/2R_\pi$ apart (the Nyquist frequency spacing). Conversely, if the range of interest of H(S) is $2S_M$, then h(s) may be sampled at intervals not greater than $s = 1/2S_M$. Thus, in equations 30 and 31, $S = 0, S_1, S_2 \ldots S_M$, and $S_M = 1/2\delta S$, the Nyquist frequency.

The modified projection ray $P1(S,\Phi)$ may be directly obtained by applying the inverse Fourier transform to the result obtained in Equation [25] or by using the convolution theorem. The inverse transform is performed in the spatial domain. The inverse transform of P(X,Y) (written symbolically in the frequency domain as P(J,I)) is just the projection itself $p(j,\phi)$.

The inverse Fourier transform of the ramp function is taken by forming an even Fourier series of the ramp function in the frequency domain and using the coefficients of the ascending terms as the inverse Fourier transform in the spatial domain. The sine term does not appear because the ramp filter is an even function in frequency space and the contributions from the negative and positive parts of the frequency spectrum account for the factor, two, multiplying the summation. In the present method, the first N_D terms of the infinite, even, Fourier series are used to approximate the convolution. The modified projection ray, $P1(S,\Phi)$ is written in terms of the original coordinates (J,I) as

$$P1(J,I) = \sum_{i_1=0}^{N_D} p(j,i_1)\, h(|i - i_1|) \qquad [32]$$

where $h(|k|)$ denotes the kth term in the even Fourier cosine series; its use has the effect of yielding a

circular convolution even though the summation is expressed monotonically and linearly. Note that h(k) is independent of angle T_j. It is useful to treat the inverse transform of the ramp filter in the light as a continuous function. This treatment is accomplished by using the integral rather than the discrete transform, or converting the summation in equation [32] to its integral analog. h(k) is expressed as

$$h(k) = 2\delta s \int_0^{(\frac{1}{2})\delta s} |S| \cos(s\pi k \delta s S)\, dS \qquad [33]$$

where δs = the increment between adjacent rays in the spatial domain. The integral in equation [33] is a truncated version of the transform of the absolute filter function with cutoffs at $S\pm_M$. Consequently, no frequencies outside the $\pm S_M$ band will be found in the convolved projection data.

This integral is solved to obtain

$$h(0) = 1/(4\delta s) \text{ for } k = 0; \qquad [34A]$$

$$h(k) = -1/\pi^2 k^2 \delta S) \text{ for } k \text{ odd}. \qquad [34B]$$

When the projection data is derived from parallel beam geometry, δs is constant. For fan beam geometry, δs varies from pixel to pixel in the reconstruction circle.

Using the explicit form of h(k), the modified projection data is solved for using the inverse Fourier two dimensional transform by writing the spatial domain convolution symbolically as

$$P1(k,\phi) = h(k) \star p(k,\phi) \qquad [35]$$

to solve the inside integral of the double integral formed by the inverse, two dimensional transform (the ★ symbolizes the convolution operation). The conceptual development leading to equation [35] is used to derive the hybrid reconstruction algorithm used in the method of the present invention. Returning to the discrete representation, the Fourier inverse transform of the ramp function, $|S|$, is written as:

$$P1(k,\phi) = p(0,\phi)/4\delta s - (1/\pi^2\delta s)\sum_{\alpha=1}^{N_D-1} p(\alpha,\phi)/(k-\alpha)^2 \quad [36]$$

where if k = odd, α = 0, 2, 4... and if k = even, α = 1,3, 5..., so $|k - \alpha|$ = odd and $(k - \alpha) \neq 0$.

If k = odd,

$$P1(k,\phi)=\{[p(k,\phi)/(4\delta s)]-[1/(\pi^2\delta s)\sum_{\alpha = 0,2,4}^{N_D-1} p(\alpha,\delta)/(k-\alpha)^2]\}. \quad [37A]$$

If k = even,

$$P1(k,\phi) = \{[p(k,\phi)/4\delta s] - [(1/2\pi^2\delta s)\sum_{\alpha=1,3,5...}^{N_D-1} p(\alpha,\phi)/(k-\alpha)^2]\} \quad [37B]$$

These two equations [37A] and [37B] complete the calculation of the inner integral in equation [35]. Completing the integration of the outer integral is accomplished by calculating the integral over ϕ. This process is traditionally called back projection.

Back projection geometry is shown in Fig. 5. The x,y increments are given by:

$$\delta x, \ \delta y = 2R_{rc}/N_p \quad [38]$$

where N_p = number of pixels in one dimension, i.e. 32, 64, 128, etc., and R_{rc} = radius of reconstruction circle 68. In similar fashion to equations [15] and [16],

$$x = -R_{rc} + (0.5 + b)\delta x \qquad [39]$$

$$y = +R_{rc} - (0.5 + c)\delta y \qquad [40]$$

and b, c = 0, 1, 2, ... $N_p - 1$.

The linear attenuation coefficient for each x,y or b,c is:

$$\mu(b,c) = \sum_{i_5=0}^{N-1} P1(j, i_5(x,y))\ \delta T1 \qquad [41]$$

where N = number of angles and $\delta T1$ is π/N for both 180 and 360 degrees of rotation. Here, $i_5(x,y)$ is determined at each angle, and j is the number of the parallel ray 50 at the projection angle j which lies closest to the point (x,y). The absorption coefficient is calculated from the following relations.

The angle ϕ of the ray of interest is defined by

$$\Phi = \tan^{-1}(y/x). \qquad [42]$$

Because ϕ is used in conjunction with T_j, ϕ must be defined in the same fashion as T_j, or from 0 to 360 degrees. If x < 0 and y >0, then $90° \leq \phi \leq 180°$. If x < 0 and y < 0, then $180° \leq \phi \leq 270°$. If x > 0 and y 0, then $270° \leq \phi \leq 360°$. Let

$$L_8 = W\ r_5 \sin\{[T_j - \phi]/[D - r_5 \cos(T_j - \phi)]\}, \qquad [43]$$

where $r_5 = (x^2 + y^2)^{1/2}$ [44]

and $i_5(x,y) = INT[L_8 + D_L/2)/(i + 0.5)]$ [45]

As before, INT[] is the "integer part of". The factor 0.5 appears in equation [45] because when $L_8 = -D_L/2$, $i_5(x,y)$ must be zero. With L_8 defined, the number of the detector corresponding to L_8 is determined using equations [6] and [45]. For example, suppose L_8 was calculated as 15.463 and the length of detector array 26, as it is in a presently preferred embodiment, was 69.12 cm with a detector aperture of 0.045 cm. The number of the detector lying on that point is given by:

$$i_5 = INT[((15.463 + 69.12)/0.045) + 0.5] = 1112.$$

This calculation indicates that the ray 50 from detector 1112 passed nearest the point (x,y) that is being reconstructed.

The quantity L_8 is defined differently for the hybrid reconstruction algorithm of the present invention than for the parallel beam geometry. At each angle, T_j, a line is passed from the x-ray target position xT_j, yT_j through the point x,y and from there to an intersection with the x-ray detector line. Thus, L_8 is defined as the distance ± from the center of the detector line. For each value of x,y, there are N back projections.

In practice, a rectangular grid with Np x Np dimensions is reconstructed and all values of absorption coefficients $\mu_{b,c}$ lying outside the circle of reconstruction 68 are set equal to zero. Using the rectangular grid for reconstruction greatly simplifies any smoothing routines when they are utilized. Further, interpolation may be used when a ray 50 does not pass through a point in the back projections.

Referring now to Fig. 6, which is a graphical representation of an exaggeration of a measured center of rotation shift for an x-ray simulator rotating 360°, the off-center shift S_j (shown at 76c) is plotted as a radius from the center of rotation 56 versus the angle in degrees. When the x-ray beam which should fall on the central detector in the detector array 26 does not pass through the center of the circle of reconstruction 68, two errors may occur. The first error is a linear displacement of the detector array 26 parallel to the central axis of the fan beam 14. The second error is the magnification or demagnification of the distance between detector arrays (δi) used in the hybrid reconstruction algorithm described above. The latter error occurs when the center of rotation 56 is shifted in a direction perpendicular to the line on which the linear detector array 26 is positioned (e.g., the detector line). Further, both errors may occur at the same time.

Referring to Fig.7, a simplified method of measuring the shift in the center of rotation is illustrated graphically. A round rod (represented schematically at reference numeral 74 in Fig. 5) which is relatively opaque to x-rays is placed at the nominal center of rotation shown by line 78 in Fig. 7A, and data obtained using the method of the present invention is shown as curve 84. An eccentricity in the center of rotation causing a shift in the direction parallel to the central axis of the projected fan beam 14 results in projection data for the rod with center shown in dotted line 80 with projection data 82. The curves 82 and 84 shown in Fig. 7A represent the reconstructed projection data taken over each angle T_j.

From this data, the shift in the number of detector widths for each angle is measured. This shift is used to correct equation [45] as follows:

$$i_s(x,y) = INT[(L_s + D_L/2]/i - s_j + 0.5] \qquad [46]$$

Where s_j is equal to the shift in number of detector widths. However, the maximum shift in either direction must be limited so that the shifted detector array 50 at the edge of detector array 26 still passes through the target object 16. As shown in Fig. 7B, when the central ray (labeled P_2) of the detector line does not pass through the center 56 of the circle of reconstruction 68, an error is introduced which blurs or distorts the image of phantom 78 as set out above. This error results, for instance, from off-center rotation of source 12 and detector array 26 through arc 66 and 27 (referring to the center point of array 26), respectively, or, in the case of a dental panoramic x-ray unit, from the superposition of rotational and translational rotation, such that the nominal center of rotation 56 is shifted to the point 57. The shift is measured and used to correct the backprojection or calculated interatively by subjective evaluation of each reconstructed image. For example, if ray P_1 at angle j is detected as ray $P_1 + 5$, it is designated $P_1 + 5$ and used to re-set the projection value at $P + 5$ and so on for P_2, ($P_2 + 5$), etc. In the application described above, the magnification or demagnification of δi is ignored.

In a presently preferred embodiment, however, the variable demagnification actually present at each row of pixels 100 (see Fig. 8) in the reconstruction circle 68 is accounted for in the reconstruction calculation. The actual variation of the Jacobian of the transformation is used in the method to apply the appropriate value of

demagnification, Magp(c), to insert the exact value of the back projected data in the calculation.

X-ray magnification is a harmonic function with the mean value M_p which can be calculated throughout the diameter of reconstruction circle 69 by the following:

$$M_p = 1/\{(1/N_p) \sum_{c=0}^{c=N_p-1} [1/Magp(c)]\} \; ; \qquad [47]$$

Fig. 4 shows the calculation of Magp(c) for 16 pixels for a circle of reconstruction with U = 100, V = 58, R_{rc} = 21.87 cm and D_{py} = 2.73 cm. For example, in pixel (7,9), the optical density 79.2 (see Fig. 11) is represented as the result of the application of projection through thirty angles into 64 detectors. Magp(c) is the scaling factor indicating demagnification caused by beam spread as one moves from the detector line towards the source 12. Magp(c) is measured at the original pixel line, c, with the source at 90° or j = 0.

Magp(c) is the Jacobian of the transformation for a coordinate system the origin of which is in the detector line with points (X′,Y′) to a coordinate system located at the pixel row c with points (X,Y). For the Jacobian,

$$J[(X,Y)/(X',Y')] = \begin{vmatrix} \delta X/\delta X' & \delta X/\delta Y' \\ \delta Y/\delta X' & \delta Y/\delta Y' \end{vmatrix} \qquad [48]$$

$$J = \begin{vmatrix} Magp(c) & 0 \\ 0 & 1 \end{vmatrix} = Magp(c). \qquad [49]$$

Thus, at the pixel line c,

$$X'_{d(i)} = X_{d(i)}\, Magp(c) \qquad [50]$$

where i is the index for the detector line and $0 \leq i \leq N_D - 1$, starting at the left side of the detector line when j = 0. This correction for the magnification resulting from the spread of the x-ray fan beam 14 can be better visualized by referring to Figs. 1, 8, and 9. As best shown in Figs. 1 and 8, the spread of x-ray beam 14 is such that the image of a target object 16 positioned closer to the detector line will be smaller than the image of a target positioned farther from the detector line. Conversely, in the back projection, demagnification must be applied to the data detected at the detector line. Consequently, the width of a detector element δi, when back projected has a dimension $\delta i' = \delta i \times Magp(c)$. A related factor occurs in treating the spacing element δr, reference numeral 110 in Fig. 9A, or 112 in Fig. 9B. This spacing element, as utilized during back projection, is either constant (Fig. 9B) or variable (Fig. 9A), the latter being preferred because it results in an orthogonal grid of pixels as shown in Fig. 8.

It is known in the art that convolution filters use a quantity δs, which is the spacing between rays, that was originally defined for parallel beam geometry. However, in the method of the present invention, the variable spacing of the rays resulting from fan beam geometry is accounted for without initially using the quantity δr as is used in parallel beam geometry. Instead, this quantity is accounted for, in conjunction with Magp(c), in scaling each row of pixels as set out above.

The ray spacing appropriate for each pixel is accounted for in the convolution using combinations of four filters, ramp, sinc, Cosine and Hamming (the functions of these four filters are shown in Fig. 11A). The method for using any of these four filters follows that set out above for the ramp filter, that is, the filter function is

convolved with the function data to produce convolved projection profiles at each pixel, and is not repeated here. The convolution filters are the Fourier, cosine series coefficients and are multiplied by the projection data to obtain the convolution profiles (see Fig. 11B). Additional description of the use of such filters for similar purposes can be found in such references as S. Webb (Ed.), The Physics of Medical Imaging, Philadelphia: Adam Hilger imprint by IOP Publishing Ltd. (1988), CHap. 4. Each of these filters has certain desired effects, and their use is selected to enhance, for instance, bone-soft tissue contrast, soft tissue, and so on as described above.

The geometry of Fig. 7B occurs, in accordance with the present invention, in a panoramic x-ray imaging apparatus in which the x-ray source and linear sensor have been adjusted to be placed within the plane of rotation.

An exemplary panoramic x-ray image apparatus is disclosed, for example, in U.S. Patent No. 5,018,177. That apparatus produces digital panoramic x-ray images of a target object by impinging an x-ray beam upon an object to be imaged and then detecting x-rays that pass through the object with a linear detector that produces a pixelized electrical signal. The x-ray source and detector are aligned with each other, and are rotated in a transverse plane about the object being imaged with the center of rotation following a curved path around the object being imaged. As the center of rotation traverses the curved path, the pixelized electrical signal is integrated during predetermined time intervals, and the integrated signal is electronically processed to produce a panoramic x-ray image of the object. To convert that apparatus from a panoramic imaging machine into a CT scanning machine, the linear radiation detector, which in this embodiment has 1024 individual detectors, is aligned horizontally, and the x-

ray beam orientation is changed from vertical to horizontal. The resultant apparatus, in accordance with the present invention, can be easily configured to facilitate changing from a vertical orientation for the x-ray source and detector for panoramic imaging, or to a horizontal orientation for CT scanning. With such an apparatus, operation in a first mode produces panoramic images, and operation in a second mode produces CT images which have been corrected for the eccentrically travelling center of rotation of the sensor and detector.

Fig. 12 presents the eccentric center of rotation geometry of Fig. 7B in more detail. Referring to Fig. 13, circle of reconstruction 101 has an origin O at coordinates 0, 0. X-ray source T is located at coordinates xt, yt and x-ray detector 102 begins at point A with coordinates xa, ya and extends to point B with coordinates xb, yb. Points K1 and K2 having respective coordinates of x1, y1 and x2, y2, are points lying on circle of reconstruction 101, and determine a line K that is parallel to detector 102. Point D, a point within detector 102, is located at coordinates xd, yd.

Several distances appearing in the geometry of Fig. 12 are also calculated including: dt which is the distance between point D on detector 102 and x-ray source T, uc[j] which is the distance between the origin O and x-ray source T; ut[j] which is equal to the distance between x-ray source T and point U in Fig. 12; ry[k] which is equal to the distance between the origin O and point K0 on the line between points K1 and K2; and rx[k] which is equal to the distance between point K1 and point K0. It should be emphasized that as x-ray source T and x-ray detector 102 rotate together, with a center of rotation following a predetermined curvilinear path, the transmission data acquired by detector 102 is read out once every

approximately 1° of rotation. In this exemplary embodiment, an entire rotation spans 231°, with each degree resulting in a different value for the geometric quantities shown schematically in Fig. 12. In addition, for each degree of rotation, a number of lines K are calculated, each line K being parallel to detector 102.

Referring now to Fig. 13 as well as Fig. 12, the method of the present invention used to correct for gross intentional eccentricities in the center of rotation is presented in flow chart form.

Beginning in block 103, for each degree j, the detector is read. Then, in block 104, the detector data is transformed to produce raw projection data. Control then passes to block 106 where the raw projection data is convolved with a ramp filter to produce filtered projection data. Control then passes to block 107 where coordinates of x-ray source T and detector D are calculated using the projection angle j and a formula used to correct for the shape of the path of the center of rotation. Specifically, for each angle j, constant "at" is defined by the equation $at = (j-26) \times \pi/180+\pi$. Constants cj and sj are then calculated as the cosine and sine, respectively, of at. These quantities are then used as correction factors in the remaining calculations. This correction is presented in more detail in the source code listing appearing in the Appendix.

Control then passes to block 108 which begins calculations involving pixel line K1 to K2. In block 109, the magnification along the pixel line K1 to K2 is calculated by dividing the distance TK by the distance TD. Then, in block 111, the coordinates of the intersection points K1 and K2 of line K with the circle of reconstruction are calculated. Control then passes to

block 112 where calculations are performed to determine the detector intersection point D1 and D2 from the projection rays from x-ray source T through K1 and from source T through point K2. Then, in block 113, the detector numbers A and B are determined which correspond to positions D1 and D2 on detector 102. Then, the functions of nested blocks 114, 116, 117 and 118 are performed whereby the contributions of the individual detector elements are calculated. Control then passes back to block 108 where processing of another pixel line is begun. After all pixel lines within the circle of reconstruction have been processed, control passes back to block 103 where the angle j is incremented, new detector data is taken, and the calculations begins again. After calculations for each angle j have been completed, control passes to block 119 where the CT numbers are calculated. Finally, in block 121, the results are displayed.

Fig. 13 is a flow chart description of the source code of the computer program in accordance with the present invention.

An alternative method used to accommodate eccentric centers of rotation will now be described. Initially, eccentricities in the rotation of x-ray tube 12 must be determined and the individual detectors comprising detector array 26 calibrated. A kit (not shown) comprised of several rods in a holder, aluminum filter, and a CT phantom can be provided for that purpose. Placing the center of the phantom for determining motion eccentricities at the nominal center of rotation 56, a scan is performed to identify any shift in the center of rotation 56. That scan also enables verification of the angle encoder output, whether that angle encoder (not shown) is integrated with the apparatus hardware (see Fig. 2) or output from those x-ray simulators which include such an encoder.

The aluminum filters are then used to determine the effective energies and x-ray output for the nominal operating voltage of the x-ray simulator. That data is used for correcting individual detector output at different voltages as at step 46. With a second phantom comprised of different materials, scans are performed at different voltages. The results are used to set up a Hounsfield scale for the different energies.

Once the initial measurements have been accomplished to load the correction algorithms into microcomputer 38 and the detectors of detector array 26 calibrated, the patient/target object 16 is positioned and the desired current and voltage parameters selected. The computer program is then initiated to acquire CT data, and on computer ready signal, x-ray output is initialized first and the x-ray rotation started. For j=0 to N, where j is the angle in degrees and N is the number of measurements (360, 720, etc.), the computer is signaled to acquire data at approximately one degree intervals (or any other odd or even increments as selected by the operator). For i=0 to N_D-1, when N_D is the number of detectors comprising detector array 26 and is operator selectable, PP(j,i) is acquired where PP(j,i) represents the output of the analog to digital converter (ADC) in microcomputer I/O board 36 for the detector i at the angle j. Note that the number of increments (angles) multiplied by the number of detectors will be the number of individual data points and that, for instance, where $0 \leq PP(j,i) \leq 4095$, 4095 corresponds to a 12 bit ADC, 8191 corresponds to a 13 bit ADC, 16,383 corresponds to a 14 bit ADC, and so on.

Each of the quantities PP(j,i) is then multiplied by a correction number obtained from the calibration procedure (step 46) to adjust the data to the values that would have been read if the individual detector were operating

The aluminum filters are then used to determine the effective energies and x-ray output for the nominal operating voltage of the x-ray simulator. That data is used for correcting individual detector output at different voltages as at step 46. With a second phantom comprised of different materials, scans are performed at different voltages. The results are used to set up a Hounsfield scale for the different energies.

Once the initial measurements have been accomplished to load the correction algorithms into microcomputer 38 and the detectors of detector array 26 calibrated, the patient/target object 16 is positioned and the desired current and voltage parameters selected. The computer program is then initiated to acquire CT data, and on computer ready signal, x-ray output is initialized first and the x-ray rotation started. For j=0 to N, where j is the angle in degrees and N is the number of measurements (360, 720, etc.), the computer is signaled to acquire data at approximately one degree intervals (or any other odd or even increments as selected by the operator). For i=0 to N_D-1, when N_D is the number of detectors comprising detector array 26 and is operator selectable, PP(j,i) is acquired where PP(j,i) represents the output of the analog to digital converter (ADC) in microcomputer I/O board 36 for the detector i at the angle j. Note that the number of increments (angles) multiplied by the number of detectors will be the number of individual data points and that, for instance, where $0 \leq PP(j,i) \leq 4095$, 4095 corresponds to a 12 bit ADC, 8191 corresponds to a 13 bit ADC, 16,383 corresponds to a 14 bit ADC, and so on.

Each of the quantities PP(j,i) is then multiplied by a correction number obtained from the calibration procedure (step 46) to adjust the data to the values that would have been read if the individual detector were operating

perfectly. This correction also remedies the beam hardening artifact as discussed above. A reference detector out is also used to correct for variation in the output of the x-ray unit as a function of the angle j.

P(j,i) is the input to the hybrid reconstruction algorithm/convolution routine (steps 47 and 48), and after convolution, Fourier artifact filters are applied as described above. For c + 0 to bp - 1 and b + 0 to N_p - 1, the back projection is done (step 38) and then repeated at the next b, next c.

Reconstructed linear attenuation coefficients are then converted to gray scale values using the Hounsfield scale derived from scanning the phantoms described above in connection with the setup procedures. A water phantom is scanned and the reconstructed coefficients are assigned 1000, with air being 0. Other values, such as for bone, are then automatically given a value in this scale. In this fashion, the Hounsfield scale is potentially wider than that of prior known CT scales, enabling detection of variations in CT values not currently available. By way of example, if the scan of a water phantom gives a value of 0.18 per cm for an average linear attenuation coefficient of water, 1000 is assigned as the value for water and 1000/.18 = 555.55 is obtained as the scale factor for the unit being used. As is known in the art, 0.36 x 5555.55, or 2000, is assigned a gray scale of 0 to represent the densest scale for this system, or twice the density of water, and 2000/255 = 7.843 is the distribution of the gray scale number vs. CT numbers:

0 CT scale = air = 255 gray scale

1000 CT scale = water = 127 gray scale

2000 CT scale = twice density of water = 0 gray scale

The CT values may be displayed along with gray scale numbers is desired.

CLAIMS:

1. In an x-ray apparatus including an x-ray source and a substantially linear x-ray detector, a method of operating the apparatus in two modes to produce both panoramic and computed tomographic images of an object, comprising:

in a first mode,

positioning said linear x-ray detector in a first plane,

rotating said x-ray detector and said x-ray source about an object and about a center of rotation in a plane of rotation transverse to said first plane while moving said center of rotation along a predetermined path,

electronically processing signals produced by said linear detector to produce a panoramic x-ray image of said object,

and in a second mode,

positioning said linear x-ray detector in said plane of rotation,

rotating said sensor and said x-ray source within said plane of rotation about an object and about a center of rotation, and

electronically processing signals produced by said linear detector to produce a computed tomographic image of said object.

2. The method of claim 1, further comprising, in said second mode, moving said center of rotation along said predetermined path.

3. The method of claim 1, said detector producing pixelized signals proportional to x-rays incident upon said detector, said step of electronically processing during said first mode comprising:

periodically integrating said pixelized signals during a series of time intervals as said center of rotation moves along said predetermined path.

4. The method of claim 3, wherein said time intervals are a function of an elapsed time required for said center of rotation to move along said predetermined path.

5. The method of claim 1, wherein said step of electronically processing during said second mode comprises:

scaling signals produced by said detector in accordance with a signal that would have been produced by said detector without said object being present;

correcting the scaled signals for magnification resulting from spread of a fan beam produced by said x-ray source;

convolving the corrected scaled signals to produce a value representing a signal that would have been

produced by the detector had the fan beam been a collimated beam; and

repeating said scaling, correcting and convolving steps at a plurality of positions as said sensor and x-ray source rotate about said object to produce a back projected image of said object.

6. The method of claim 2, wherein said step of electronically processing during said second mode comprises correcting the signals produced by the detector for distortion from movement of said center of rotation along said predetermined path.

7. A method of operating an x-ray apparatus to computed tomographic images of the maxillo facial area of a patient, comprising:

in a first mode,

generating an x-ray fan beam in a substantially vertical plane,

rotating said x-ray fan beam in a substantially horizontal plane about a maxillo facial target area while translating said fan beam along a curvilinear path,

detecting an intensity of x-rays in said substantially vertical plane after said x-rays have passed through said maxillo facial target area to produce a detected intensity, and

calculating a panoramic image of a maxillo facial area of a patient in said maxillo facial target area from said detected intensity, and

in a second mode,

generating an x-ray fan beam in said substantially horizontal plane,

rotating said x-ray fan beam in said substantially horizontal plane about said maxillo facial target area while translating said fan beam along said curvilinear path,

detecting an intensity of x-rays in said substantially horizontal plane after said x-rays have passed through said maxillo facial target area, to produce a detected intensity, and

correcting said detected intensity for said curvilinear path to produce a corrected intensity, and

calculating a computed tomographic image of said maxillo facial area of said patient in said maxillo facial target area from said corrected intensity.

8. An x-ray imaging apparatus for producing both panoramic images and computed tomographic images, comprising:

an x-ray source positionable to produce an x-ray in fan beam in first and second orthogonal planes;

a linear x-ray detector for detecting x-rays produced by said x-ray source at a substantially fixed distance from said x-ray source and for producing signals indicative of an intensity of x-rays incident on said detector, said detector being positionable in said first and second orthogonal planes;

means for rotating said source and detector together in said first plane about a center of rotation located in said first plane;

means for moving said center of rotation along a curvilinear path while said source and detector rotate; and

a signal processor for calculating, from detected x-ray intensity, a panoramic image of an object located near said center of rotation when said x-ray fan beam and said detector both lie in said second plane, and for calculating a computed tomographic image of an object located near said center of rotation when said x-ray fan beam and said detector both lie in said first plane.

9. The apparatus of claim 8, said linear x-ray detector comprising individual detecting elements.

10. The apparatus of claim 9, said linear x-ray detector comprising 1024 individual detecting elements.

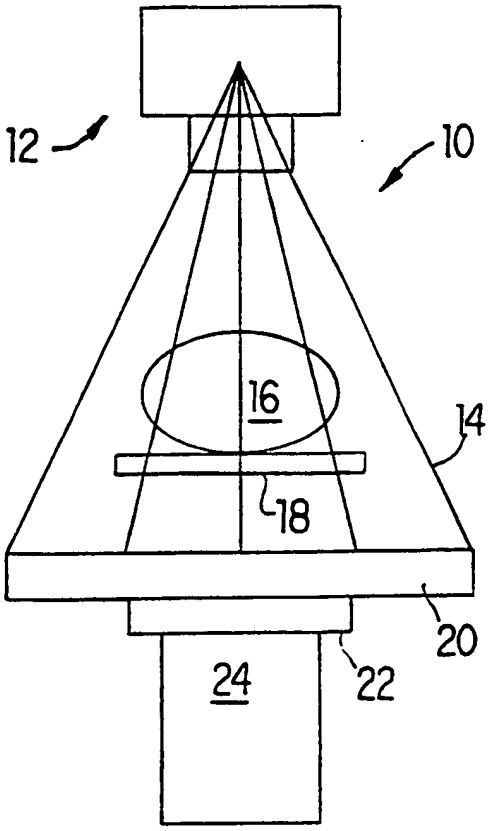

FIG. 1

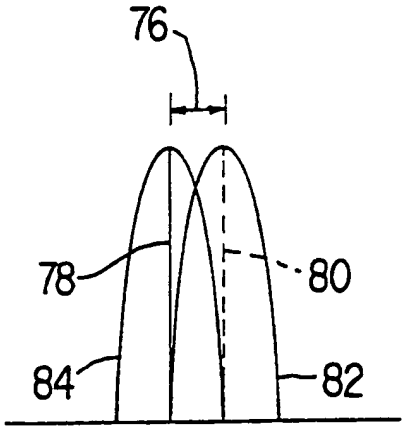

FIG. 7A

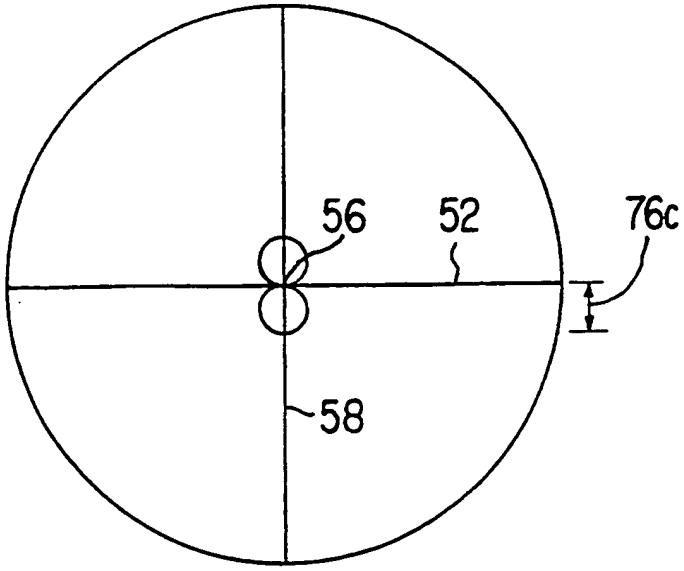

FIG. 6

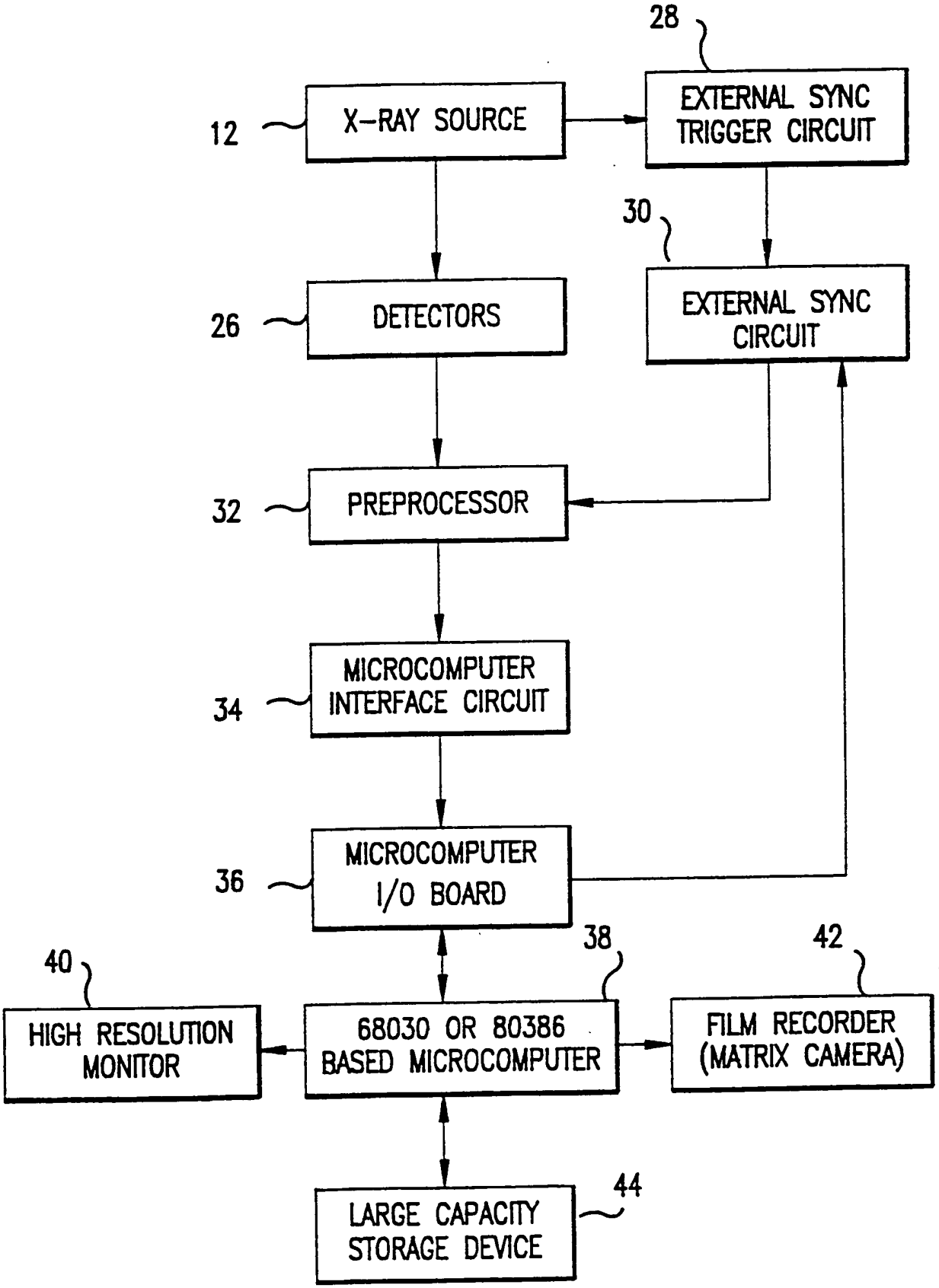
28
EXTERNAL SYNC TRIGGER CIRCUIT
12
X-RAY SOURCE
30
EXTERNAL SYNC CIRCUIT
26
DETECTORS
32
PREPROCESSOR
34
MICROCOMPUTER INTERFACE CIRCUIT
36
MICROCOMPUTER I/O BOARD
40
HIGH RESOLUTION MONITOR
38
68030 OR 80386 BASED MICROCOMPUTER
42
FILM RECORDER (MATRIX CAMERA)
44
LARGE CAPACITY STORAGE DEVICE

FIG.2

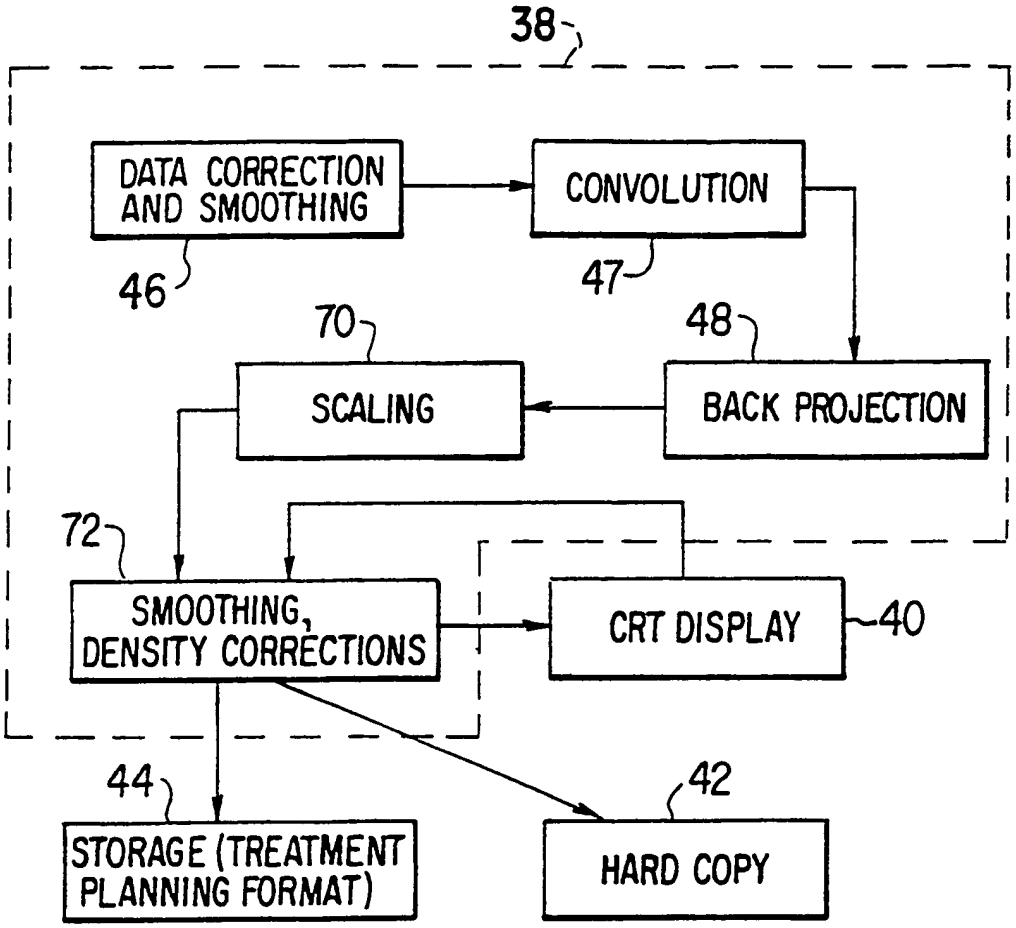

FIG. 3

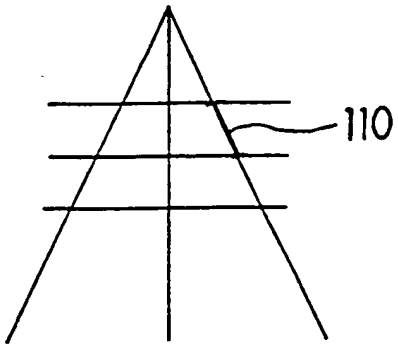

FIG. 9A

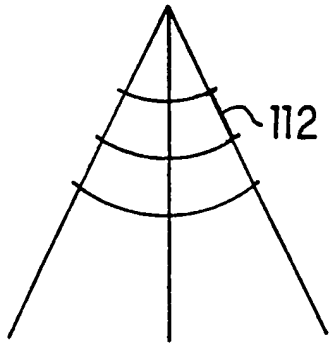

FIG. 9B

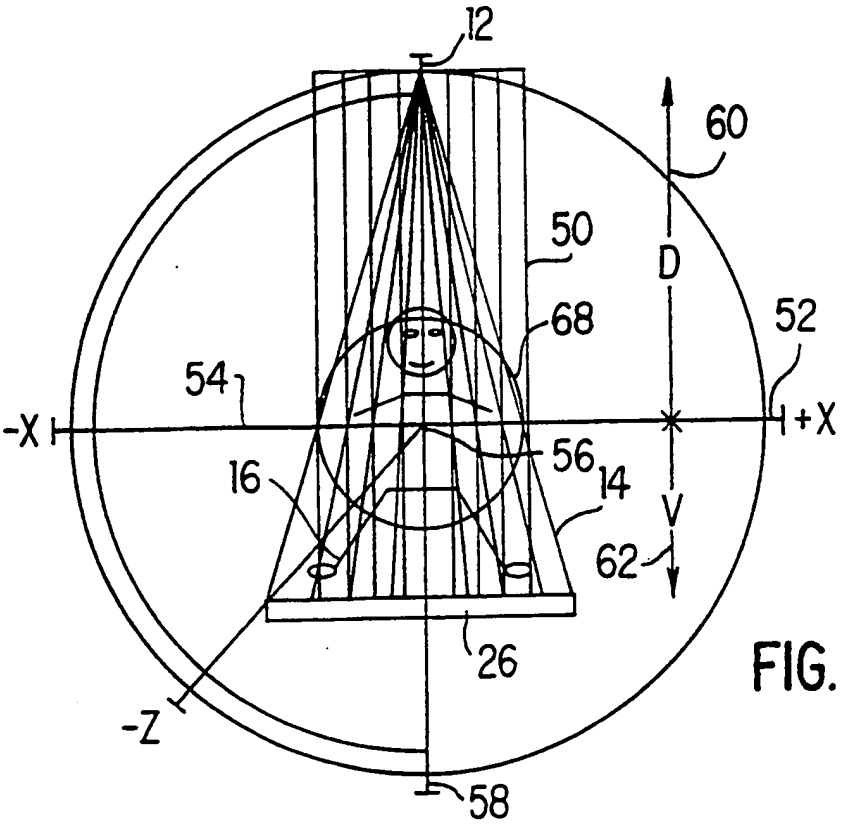

FIG. 4

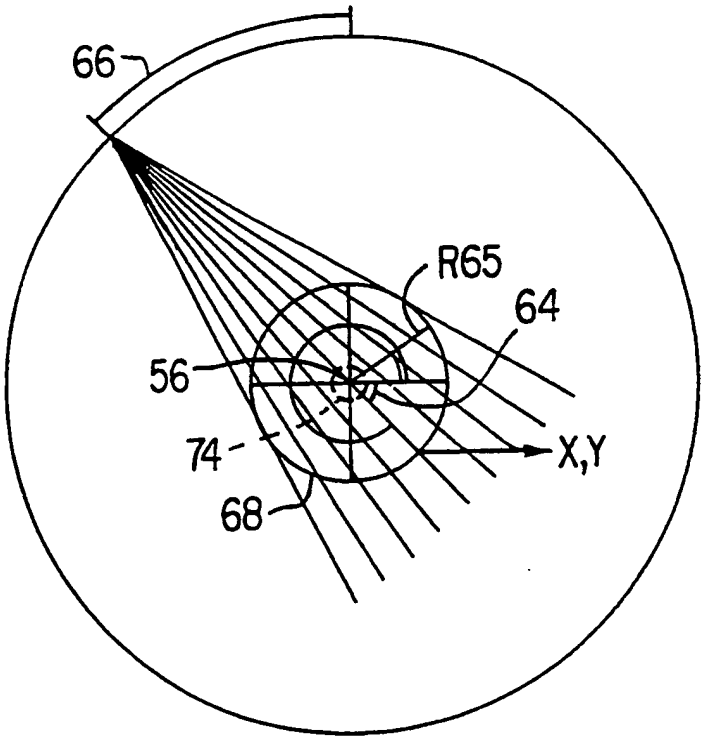

FIG. 5

C	MAGP(C)
0	0.503
1	0.520
2	0.537
3	0.555
4	0.572
5	0.589
6	0.606
7	0.624
8	0.641
9	0.658
10	0.676
11	0.693
12	0.710
13	0.728
14	0.745
15	0.762

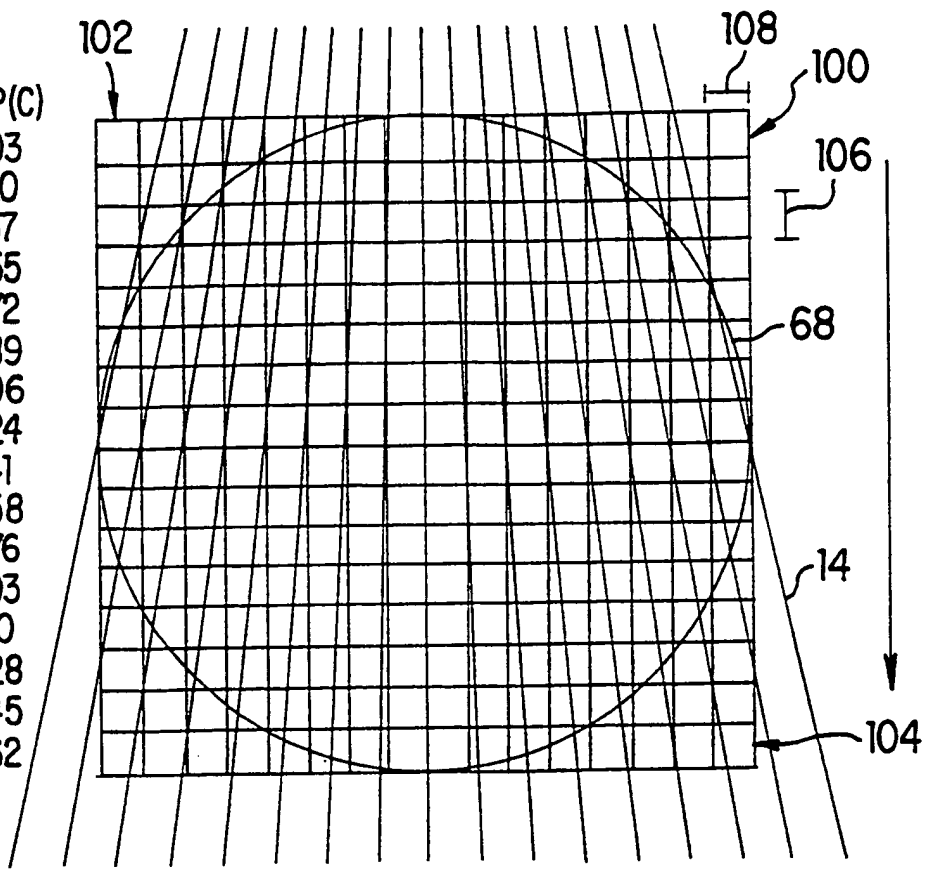

FIG. 8

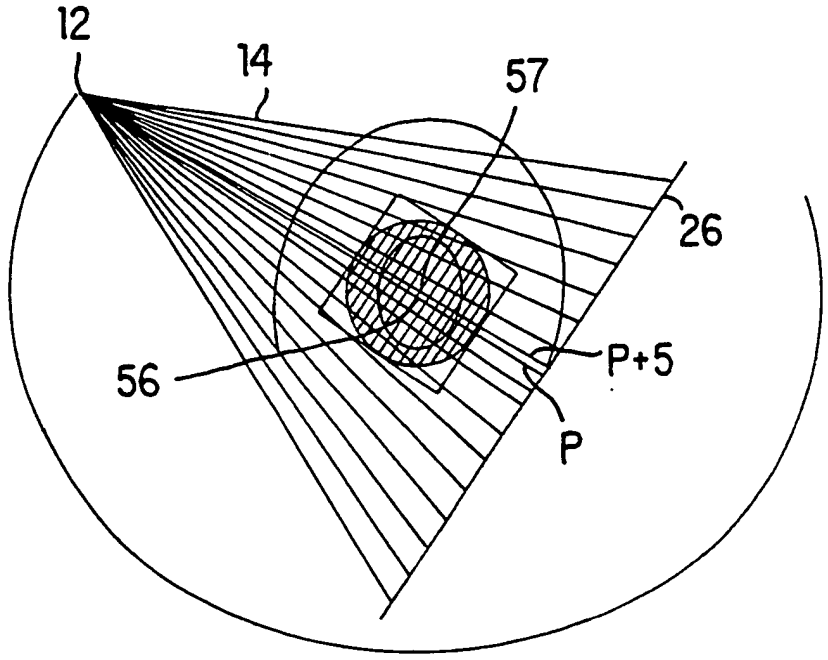

FIG. 7B

	0	1	2	3	4	5	6	7	8	9	10	11	12	13	14	15
0	*	*	*	*	*	*	*	*	*	*	*	*	*	*	*	*
1	*	*	*	*	*	*	*	*	*	*	*	*	*	*	*	*
2	*	*	*	*	*	*	*	*	*	*	*	*	*	*	*	*
3	*	*	*	*	*	*	*	*	*	*	*	*	*	*	*	*
4	*	*	*	*	*	77.1	75.7	72.3	74.3	73.7	75.8	77.1	*	*	*	*
5	*	*	*	75.2	76.2	71.9	82.4	73.2	79.8	73.2	83.1	71.3	76.3	75.9	*	*
6	*	*	72.6	76.3	78.7	79.3	74.0	76.1	77.0	76.1	74.7	79.4	78.8	75.7	72.6	*
7	*	*	77.4	71.5	76.8	75.8	76.1	79.2	74.8	79.2	76.1	75.9	76.8	71.6	77.4	*
8	*	*	81.3	73.0	80.7	73.3	77.2	74.8	72.4	72.3	76.0	73.4	80.7	73.1	81.4	*
9	*	*	77.4	71.5	76.8	75.8	76.0	79.1	75.5	79.2	76.1	75.9	76.2	71.6	77.4	*
10	*	*	72.6	76.3	78.7	79.3	74.7	76.0	76.5	76.1	74.7	78.8	79.4	76.4	72.1	*
11	*	*	*	75.2	76.2	71.9	83.1	72.6	79.9	73.2	82.6	72.5	75.7	75.2	*	*
12	*	*	*	*	*	77.1	75.7	73.1	74.3	73.7	75.8	76.6	*	*	*	*
13	*	*	*	*	*	*	*	*	*	*	*	*	*	*	*	*
14	*	*	*	*	*	*	*	*	*	*	*	*	*	*	*	*
15	*	*	*	*	*	*	*	*	*	*	*	*	*	*	*	*

FIG.10

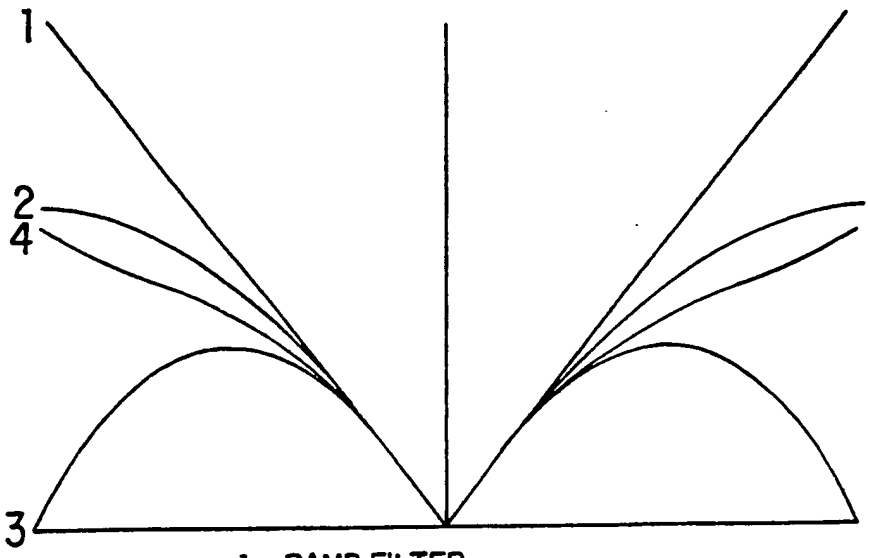

1- RAMP FILTER
2- SHEPP-LOGAN SINC FILTER
3- COSINE LOW PASS FILTER
4- HAMMING COSINE LOW PASS FILTER

FIG. 11A

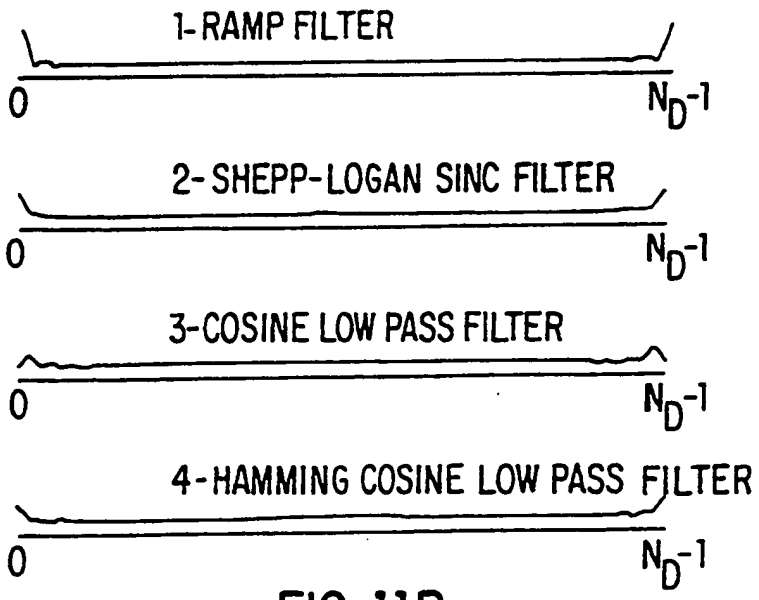

FIG. 11B

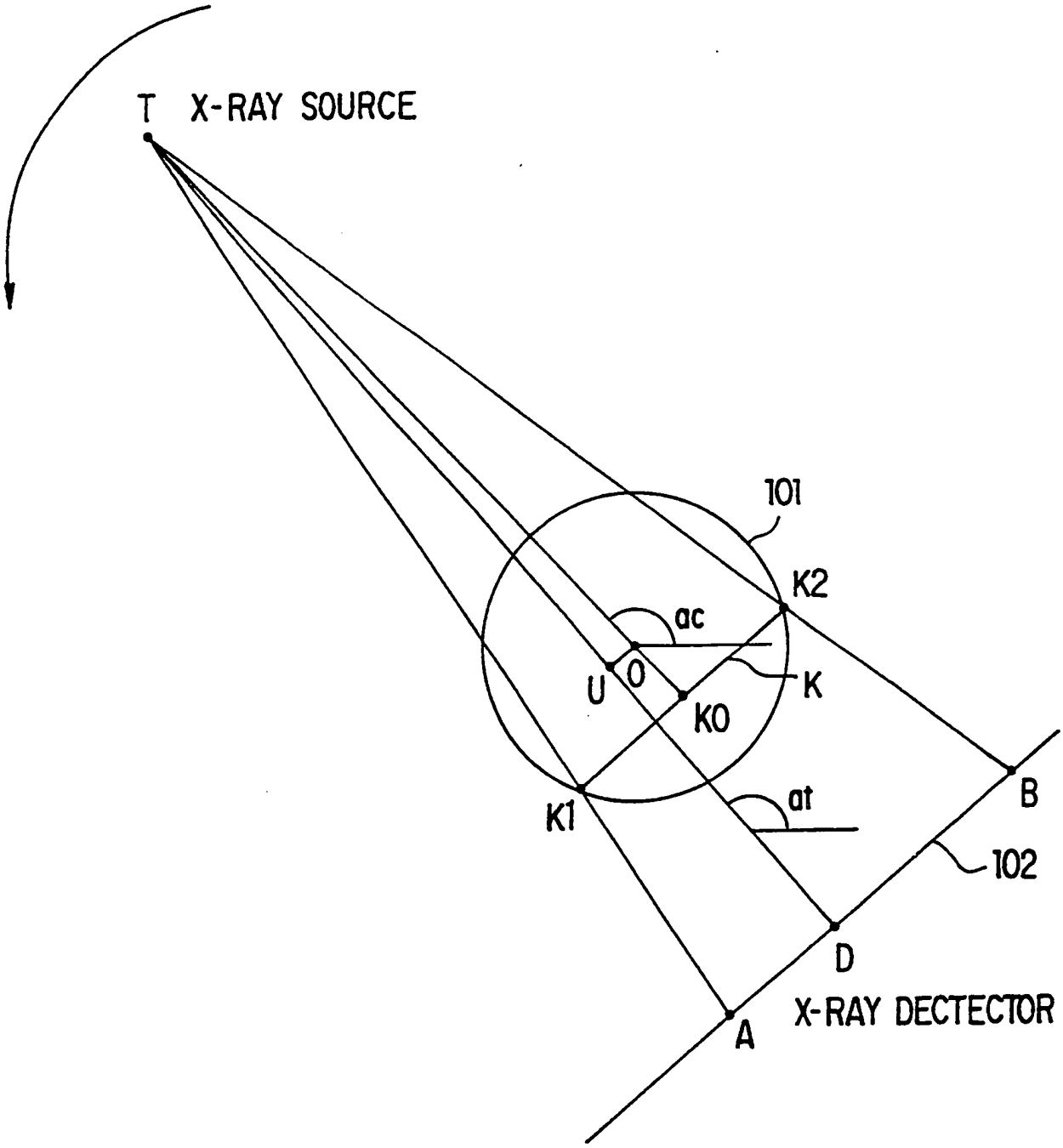

FIG. 12

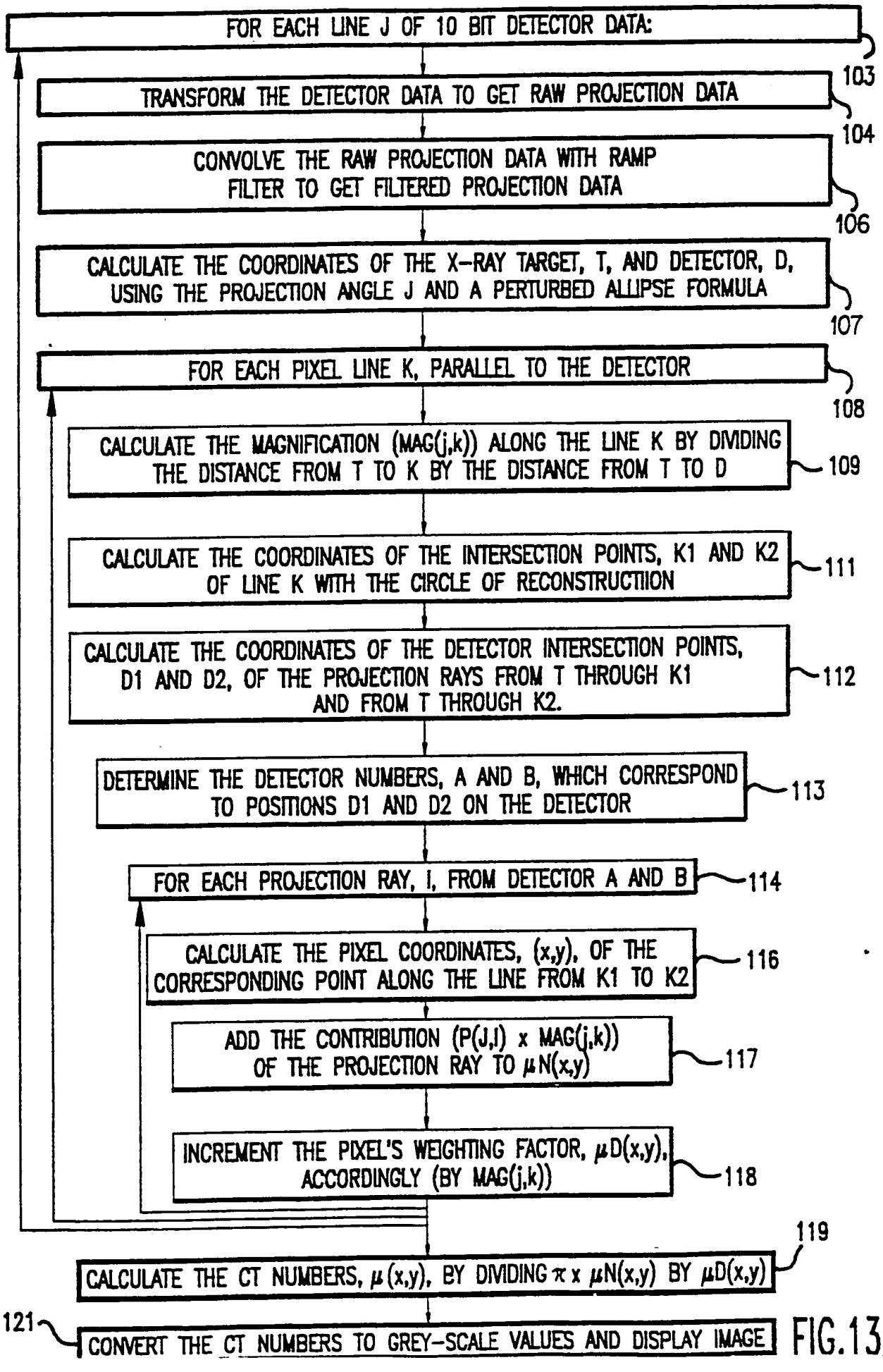
FOR EACH LINE J OF 10 BIT DETECTOR DATA:
103
TRANSFORM THE DETECTOR DATA TO GET RAW PROJECTION DATA
104
CONVOLVE THE RAW PROJECTION DATA WITH RAMP FILTER TO GET FILTERED PROJECTION DATA
106
CALCULATE THE COORDINATES OF THE X-RAY TARGET, T, AND DETECTOR, D, USING THE PROJECTION ANGLE J AND A PERTURBED ALLIPSE FORMULA
107
FOR EACH PIXEL LINE K, PARALLEL TO THE DETECTOR
108
CALCULATE THE MAGNIFICATION (MAG(j,k)) ALONG THE LINE K BY DIVIDING THE DISTANCE FROM T TO K BY THE DISTANCE FROM T TO D
109
CALCULATE THE COORDINATES OF THE INTERSECTION POINTS, K1 AND K2 OF LINE K WITH THE CIRCLE OF RECONSTRUCTIION
111
CALCULATE THE COORDINATES OF THE DETECTOR INTERSECTION POINTS, D1 AND D2, OF THE PROJECTION RAYS FROM T THROUGH K1 AND FROM T THROUGH K2.
112
DETERMINE THE DETECTOR NUMBERS, A AND B, WHICH CORRESPOND TO POSITIONS D1 AND D2 ON THE DETECTOR
113
FOR EACH PROJECTION RAY, I, FROM DETECTOR A AND B
114
CALCULATE THE PIXEL COORDINATES, (x,y), OF THE CORRESPONDING POINT ALONG THE LINE FROM K1 TO K2
116
ADD THE CONTRIBUTION (P(J,I) x MAG(j,k)) OF THE PROJECTION RAY TO μN(x,y)
117
INCREMENT THE PIXEL'S WEIGHTING FACTOR, μD(x,y), ACCORDINGLY (BY MAG(j,k))
118
119
CALCULATE THE CT NUMBERS, μ(x,y), BY DIVIDING π x μN(x,y) BY μD(x,y)
121
CONVERT THE CT NUMBERS TO GREY-SCALE VALUES AND DISPLAY IMAGE

FIG.13

I. CLASSIFICATION OF SUBJECT MATTER (if several classification symbols apply, indicate all)[6]

According to International Patent Classification (IPC) or to both National Classification and IPC

Int.Cl.5 A 61 B 6/02 . A 61 B 6/03

II. FIELDS SEARCHED

Minimum Documentation Searched[7]

Classification System	Classification Symbols
Int.Cl.5	A 61 B

Documentation Searched other than Minimum Documentation to the Extent that such Documents are Included in the Fields Searched[8]

III. DOCUMENTS CONSIDERED TO BE RELEVANT[9]

Category °	Citation of Document,[11] with indication, where appropriate, of the relevant passages[12]	Relevant to Claim No.[13]
A	US,A,4365339 (J.M. PAVKOVICH et al.) 21 December 1982, see figures 1-3; column 8, line 62 - column 11, line 2; column 12, lines 31-46; claim 1 (cited in the application) ---	1,8
P,A	DE,A,4133066 (KAB. K. MORITA S.) 9 April 1992, see column 1, line 65 - column 3, line 16; column 4, lines 7-37; claims 1,2; figures 1,3,5 -----	1,8

° Special categories of cited documents :[10]

"A" document defining the general state of the art which is not considered to be of particular relevance

"E" earlier document but published on or after the international filing date

"L" document which may throw doubts on priority claim(s) or which is cited to establish the publication date of another citation or other special reason (as specified)

"O" document referring to an oral disclosure, use, exhibition or other means

"P" document published prior to the international filing date but later than the priority date claimed

"T" later document published after the international filing date or priority date and not in conflict with the application but cited to understand the principle or theory underlying the invention

"X" document of particular relevance; the claimed invention cannot be considered novel or cannot be considered to involve an inventive step

"Y" document of particular relevance; the claimed invention cannot be considered to involve an inventive step when the document is combined with one or more other such documents, such combination being obvious to a person skilled in the art.

"&" document member of the same patent family

IV. CERTIFICATION

Date of the Actual Completion of the International Search	Date of Mailing of this International Search Report
07-10-1992	04 NOV 1992
International Searching Authority	**Signature of Authorized Officer**
EUROPEAN PATENT OFFICE	E. H. Ludwig

Box I Observations where certain claims were found unsearchable (Continuation of item 1 of first sheet)

This international search report has not been established in respect of certain claims under Article 17(2)(a) for the following reasons:

1. [X] Claims Nos.: 7
because they relate to subject matter not required to be searched by this Authority, namely:

(Methods for treatment of the human or animal body by surgery or therapy, as well as diagnostic methods) Rule 39.1. (iv) PCT

2. [ ] Claims Nos.:
because they relate to parts of the international application that do not comply with the prescribed requirements to such an extent that no meaningful international search can be carried out, specifically:

3. [ ] Claims Nos.:
because they are dependent claims and are not drafted in accordance with the second and third sentences of Rule 6.4(a).

Box II Observations where unity of invention is lacking (Continuation of item 2 of first sheet)

This International Searching Authority found multiple inventions in this international application, as follows:

1. [ ] As all required additional search fees were timely paid by the applicant, this international search report covers all searchable claims.

2. [ ] As all searchable claims could be searches without effort justifying an additional fee, this Authority did not invite payment of any additional fee.

3. [ ] As only some of the required additional search fees were timely paid by the applicant, this international search report covers only those claims for which fees were paid, specifically claims Nos.:

4. [ ] No required additional search fees were timely paid by the applicant. Consequently, this international search report is restricted to the invention first mentioned in the claims; it is covered by claims Nos.:

Remark on Protest

[ ] The additional search fees were accompanied by the applicant's protest.

[ ] No protest accompanied the payment of additional search fees.

ANNEX TO THE INTERNATIONAL SEARCH REPORT ON INTERNATIONAL PATENT APPLICATION NO. US 9205218 SA 61715

This annex lists the patent family members relating to the patent documents cited in the above-mentioned international search report. The members are as contained in the European Patent Office EDP file on 27/10/92
The European Patent Office is in no way liable for these particulars which are merely given for the purpose of information.

Patent document cited in search report	Publication date	Patent family member(s)	Publication date
US-A- 4365339	21-12-82	US-A- 4149247	10-04-79
		CA-A- 1111573	27-10-81
		DE-A,C 2657895	14-07-77
		FR-A,B 2336690	22-07-77
		GB-A- 1577015	15-10-80
		GB-A- 1577016	15-10-80
		GB-A- 1577014	15-10-80
		JP-A- 52079894	05-07-77
		NL-A- 7614230	27-06-77
		SE-A- 7614458	24-06-77
DE-A- 4133066	09-04-92	JP-A- 4144548	19-05-92